How well do state-of-the-art techniques measuring the vertical profile of tropospheric aerosol extinction compare?

B. Schmid,[1] R. Ferrare,[2] C. Flynn,[3] R. Elleman,[4] D. Covert,[4] A. Strawa,[5] E. Welton,[6] D. Turner,[3,7] H. Jonsson,[8] J. Redemann,[1] J. Eilers,[5] K. Ricci,[9] A. G. Hallar,[5] M. Clayton,[10] J. Michalsky,[11] A. Smirnov,[12] B. Holben,[6] and J. Barnard[3]

Received 3 February 2005; revised 6 July 2005; accepted 27 July 2005; published 1 February 2006.

[1] The recent Department of Energy Atmospheric Radiation Measurement (ARM) Aerosol Intensive Operations Period (AIOP, May 2003) yielded one of the best measurement sets obtained to date to assess our ability to measure the vertical profile of ambient aerosol extinction $\sigma_{ep}(\lambda)$ in the lower troposphere. During one month, a heavily instrumented aircraft with well-characterized aerosol sampling ability carrying well-proven and new aerosol instrumentation devoted most of the 60 available flight hours to flying vertical profiles over the heavily instrumented ARM Southern Great Plains (SGP) Climate Research Facility (CRF). This allowed us to compare vertical extinction profiles obtained from six different instruments: airborne Sun photometer (AATS-14), airborne nephelometer/absorption photometer, airborne cavity ring-down system, ground-based Raman lidar, and two ground-based elastic backscatter lidars. We find the in situ measured $\sigma_{ep}(\lambda)$ to be lower than the AATS-14 derived values. Bias differences are 0.002–0.004 Km^{-1} equivalent to 13–17% in the visible, or 45% in the near-infrared. On the other hand, we find that with respect to AATS-14, the lidar $\sigma_{ep}(\lambda)$ are higher: Bias differences are 0.004 Km^{-1} (13%) and 0.007 Km^{-1} (24%) for the two elastic backscatter lidars (MPLNET and MPLARM, λ = 523 nm) and 0.029 Km^{-1} (54%) for the Raman lidar (λ = 355 nm). An unnoticed loss of sensitivity of the Raman lidar had occurred leading up to AIOP, and we expect better agreement from the recently restored system. Looking at the collective results from six field campaigns conducted since 1996, airborne in situ measurements of $\sigma_{ep}(\lambda)$ tend to be biased slightly low (17% at visible wavelengths) when compared to airborne Sun photometer $\sigma_{ep}(\lambda)$. On the other hand, $\sigma_{ep}(\lambda)$ values derived from lidars tend to have no or positive biases. From the bias differences we conclude that the typical systematic error associated with measuring the tropospheric vertical profile of the ambient aerosol extinction with current state-of-the-art instrumentation is 15–20% at visible wavelengths and potentially larger in the UV and near-infrared.

Citation: Schmid, B., et al. (2006), How well do state-of-the-art techniques measuring the vertical profile of tropospheric aerosol extinction compare?, *J. Geophys. Res.*, *111*, D05S07, doi:10.1029/2005JD005837.

1. Introduction

[2] A major uncertainty in predicting future changes to the Earth system in general, and its climate in particular, stems from the difficulty of modeling the effects of atmospheric aerosols. In fact, recent modeling studies debate to what extent controlling the emission of aerosol (i.e., reducing the emission of light-absorbing aerosol) into the Earth's atmosphere may be a feasible way to slow global warming [*Jacobson*, 2002; *Hansen et al.*, 2000; *Sato et al.*, 2003; *Penner et al.*, 2003; *Penner*, 2003]. The current low confidence in the estimates of aerosol induced perturbations of the Earth's radiation balance is caused by the highly nonuniform compositional, spatial and temporal distribution of tropospheric aerosols owing to their heterogeneous sources and short lifetimes.

[1]Bay Area Environmental Research Institute, Sonoma, California, USA.
[2]NASA Langley Research Center, Hampton, Virginia, USA.
[3]Pacific Northwest National Laboratory, Richland, Washington, USA.
[4]Department of Atmospheric Sciences, University of Washington, Seattle, Washington, USA.
[5]NASA Ames Research Center, Moffett Field, California, USA.
[6]NASA Goddard Space Flight Center, Greenbelt, Maryland, USA.
[7]Now at Space Science and Engineering Center, University of Wisconsin, Madison, Wisconsin, USA.
[8]Center for Interdisciplinary Remotely-Piloted Aircraft Studies, Marina, California, USA.
[9]Los Gatos Research Inc., Mountain View, California, USA.
[10]SAIC/NASA Langley Research Center, Hampton, Virginia, USA.
[11]NOAA Air Resources Laboratory, Boulder, Colorado, USA.
[12]Goddard Earth Science and Technology Center, University of Maryland Baltimore County/NASA Goddard Space Flight Center, Greenbelt, Maryland, USA.

Copyright 2006 by the American Geophysical Union.
0148-0227/06/2005JD005837$09.00

[3] Aerosols affect climate through a variety of pathways. These pathways include direct effects on the scattering and absorption of radiation, indirect effects caused by aerosol roles in cloud microphysics, and "semidirect" effects caused by aerosol modification of atmospheric heating, temperature profiles, convection, and large-scale horizontal transport [e.g., *Ackerman et al.*, 2000; *Chameides and Bergin*, 2002; *Lelieveld et al.*, 2002; *Menon et al.*, 2002]. Many of these pathways can affect precipitation, and thus aerosols are intimately linked to the hydrological cycle [e.g., *Ramanathan et al.*, 2001; *Rotstayn and Lohmann*, 2002].

[4] Monitoring the global distribution of aerosols requires the combination of continuous observations from satellites, networks of ground-based instruments, and dedicated field experiments [*Kaufman et al.*, 2002].

[5] The globally distributed Aerosol Robotic Network (AERONET) consisting of ~200 Sun-and sky-scanning ground-based automated radiometers provides column measurements of aerosol optical properties, with up to ten years of observations in some locations [*Holben et al.*, 2001]. These data are used extensively for the validation of satellite-derived aerosol properties [e.g., *Diner et al.*, 2001; *Torres et al.*, 2002; *Chu et al.*, 2003]. In situ measurements of aerosol optical properties and composition are made by numerous ground-based networks around the world [e.g., *Delene and Ogren*, 2002; *VanCuren*, 2003]. Ground-based lidar networks monitoring the vertical distribution of aerosols are also emerging [*Welton et al.*, 2001; *Ansmann et al.*, 2003]. The era of continuous satellite-based observation of the vertical distribution of tropospheric aerosols has begun very recently with the launch of the Geoscience Laser Altimeter System (GLAS) in January 2003 [*Spinhirne et al.*, 2005].

[6] Here, we assess the accuracy with which the vertical profile of aerosol extinction (a fundamental aerosol property) can currently be measured with state-of-the-art instrumentation. We cannot stress enough that for climate considerations it is the properties of the unaltered aerosol at its ambient concentration and thermodynamic state that are of interest. Hence the accuracy assessment presented here applies to the measurement of the vertical profile of ambient aerosol extinction. To arrive at this assessment we rely on comparisons of ambient aerosol extinction profiles obtained in coordinated field campaigns that include in situ and remote sensing measurements of aerosols aboard airborne platforms over surface-based lidars. We start with the results of a recent campaign, the Department of Energy Atmospheric Radiation Measurement (ARM) Aerosol Intensive Operations Period (AIOP, May 2003), and then consider these results in the context of findings from other field campaigns conducted since 1996.

[7] AIOP yielded one of the best suited measurement sets obtained to date to assess our ability to measure the vertical profile of ambient aerosol extinction. During one month, a heavily instrumented aircraft with well-characterized aerosol sampling ability carrying a combination of well-proven and new aerosol instrumentation, devoted most of the 60 available flight hours to flying vertical profiles over the heavily instrumented ARM Southern Great Plains (SGP) Climate Research Facility (CRF) [*Ackerman and Stokes*, 2003]. This allows us to compare vertical extinction profiles obtained from 6 different instruments: airborne Sun photometer, airborne nephelometer/absorption photometer, airborne cavity ring-down system, ground-based Raman lidar and 2 ground-based elastic backscatter lidars.

2. Measurements

2.1. Airborne Measurements

2.1.1. Twin Otter Aircraft

[8] The Twin Otter is operated by the Marina, California, based Center for Interdisciplinary Remotely Piloted Aircraft Studies (CIRPAS) [*Bluth et al.*, 1996; *Bane et al.*, 2004]. Between 6 and 29 May 2003, the Twin Otter performed 16 research flights out of Ponca City, Oklahoma, Airport. All flight patterns were anchored at the ARM SGP CRF (36.60°N, 97.48°W, 319 m), 32 km west of Ponca City. For the AIOP campaign the maximum flight altitude was 5.6 km. All in situ instrumentation aboard the Twin Otter discussed here sampled aerosol from a shrouded intake whose inlet passing efficiency was tested in airborne and wind tunnel experiments by *Hegg et al.* [2005]. They find no appreciable loss in efficiency for particles smaller than ~3.5 μm diameter at the typical Twin Otter velocity of 50 m s^{-1}. For larger particles, the efficiency decreases rapidly but levels off at an efficiency of slightly better than 0.6 for particles 5.5 μm diameter through the limit of their measurements at 9 μm.

2.1.2. Aerosol Extinction From Sun Photometry Aboard the Twin Otter

[9] The NASA Ames Airborne Tracking 14-channel Sun photometer (AATS-14) measures the transmission of the direct solar beam in 14 spectral channels (354 to 2139 nm). AATS-14 is an enhanced version of the AATS-6 instrument [*Matsumoto et al.*, 1987].

[10] The AATS-14 tracking head is mounted outside the aircraft skin to minimize blockage by aircraft structures and to avoid data contamination by aircraft window effects. The instrument locates and tracks the Sun without input from an operator and records data in a self-contained data system. Using aircraft-provided data on latitude, longitude and ambient static pressure, aerosol (or particulate) optical depth $\tau_p(\lambda)$ and columnar water vapor (CWV) are computed and displayed in real time.

[11] AATS-14 made its first science flights during the Tropospheric Aerosol Radiative Forcing Observational Experiment (TARFOX) in July 1996 [*Russell et al.*, 1999a, 1999b]. Since then, AATS-14 has been operated on many aircraft in numerous aerosol oriented field experiments: ACE-2 [*Schmid et al.*, 2000], SAFARI 2000 [*Schmid et al.*, 2003a], ACE-Asia [*Schmid et al.*, 2003b], CLAMS [*Redemann et al.*, 2005], SOLVE-2 [*Livingston et al.*, 2005; *Russell et al.*, 2005]), and ADAM [*Bucholtz et al.*, 2003].

[12] During AIOP, AATS-14 operated successfully on all 16 Twin Otter research flights. Conditions in the boundary layer tended to be relatively turbulent, resulting in larger (compared to flights over the ocean surface) AATS-14 tracking errors. Measurements exceeding a tracking error of 1° were flagged as questionable data points and not used for this study. The tracking capabilities of AATS-14 under such bumpy conditions have recently been improved by changing settings in the tracking software. To avoid contamination of the AATS-14 entrance window, the tracking

head was moved into its park position before flying through clouds.

[13] Our methods for data reduction, calibration, and error analysis have been described previously [*Russell et al.*, 1993a; *Schmid and Wehrli*, 1995; *Schmid et al.*, 1998, 2001]. A brief summary is given here. The AATS-14 channels are chosen to allow separation of aerosol, water vapor, and ozone transmission. From these slant-path transmissions we retrieve $\tau_p(\lambda)$ in 13 narrow wavelength bands and the columnar amounts of water vapor and ozone. In addition to the corrections for Rayleigh scattering and O_3 absorption, some channels require corrections for NO_2, H_2O and O_2-O_2 absorption. Cross sections were computed using LBLRTM 6.01 [*Clough and Iacono*, 1995] with the CKD 2.4.1 continuum model using the HITRAN 2000 (v 11.0) line list [*Rothman et al.*, 2001; *Rothman and Schroeder*, 2002] (including an update for water vapor from 04/2001, see http://www.hitran.com/hitran/updates.html). NO_2 cross sections not included in LBLRTM 6.01 were taken from *Harder et al.* [1997]. NO_2 was assumed constant at 2×10^{-15} molecules cm^{-2}.

[14] The AIOP AATS-14 data set consists of 13 wavelengths (354, 380, 453, 499, 519, 604, 675, 778, 865, 1019, 1241, and 2139 nm) at which we retrieve $\tau_p(\lambda)$ and the 941-nm wavelength, which we use to determine CWV [*Schmid et al.*, 2001].

[15] The columnar O_3 content needed to correct for O_3 absorption was derived from high-altitude (hence low-$\tau_p(\lambda)$) spectra (discussed below) by using the spectral fitting technique introduced by *King and Byrne* [1976] and validated recently by *Livingston et al.* [2005]. The so-determined columnar O_3 content $O_3(z_i)$ corresponds to the flight altitude z_i, at which the low-$\tau_p(\lambda)$ spectra were measured. Values at all other flight altitudes were determined by scaling a standard O_3 profile so it passes through $O_3(z_i)$.

[16] AATS-14 was calibrated at the Mauna Loa Observatory (MLO), Hawaii, 1.5 months before and 1.5 months after the AIOP campaign using the Langley plot technique [*Schmid and Wehrli*, 1995]. As a result of band pass filter degradation, the calibration constants obtained from the postmission calibration were slightly different from those obtained from the premission calibration. None of the 14 calibration constants had changed by more than 1.6% with 5 channels exhibiting a change of less than 0.5%.

[17] To determine the best calibration constants, $V_0(\lambda)$, applicable to the AIOP data set we inspected spectra with low $\tau_p(\lambda)$ values measured during higher-altitude legs. This resulted in 16 spectra taken during 14 flights with $\tau_p(\lambda)$ between 0.01 and 0.06 (at 499 nm) at altitudes 3.1–5.6 km. Starting with calibration constants obtained by linearly interpolating $V_0(\lambda)$ between premission and postmission calibration, we then adjusted the calibration constants within the bounds of premission and postmission calibration in such a fashion that the retrieved $\tau_p(\lambda)$ yielded "smooth" $\tau_p(\lambda)$ spectra for all 16 high-altitude cases. This procedure revealed that it is best to use slightly different calibration constants for different periods within the AIOP period. This fine-tuning of the calibration constants indicates that some of the optical filters must have degraded in a stepwise fashion.

[18] During AIOP, AATS-14 sampled at 3 Hz with data recorded every 4 s consisting of an average of nine samples taken in the first 3 of the 4 s. The sample standard deviation of all science detector outputs is also stored in the data files. These standard deviations were used in our cloud-screening algorithm that is based on clouds exhibiting higher standard deviations than clear sky. This cloud-screening method can be ambiguous when thick and highly variable dust layers are present above the aircraft. However, we did not encounter such conditions during AIOP.

[19] Because Sun photometers have a nonzero field of view (FOV), they measure some diffuse light in addition to the direct solar beam. As a result, uncorrected Sun photometer measurements can overestimate direct beam transmission and hence underestimate $\tau_p(\lambda)$. For most aerosol conditions and Sun photometer FOVs these effects are negligible. For example, *Eck et al.* [1999] report that for the AERONET Sun/sky radiometers, which have FOV half angle 0.6°, the diffuse light correction to apparent $\tau_p(\lambda)$ is <0.7% of $\tau_p(\lambda)$, even for desert dust with aerosol effective radius as large as 1.75 μm. AATS-6 and -14, are designed and built with a relatively large FOV (measured half angle 1.85°) to help keep the full solar disk in view when Sun tracking during aircraft maneuvers. This larger FOV makes it necessary to assess quantitatively the diffuse light effects on AATS-derived $\tau_p(\lambda)$ when large particles are dominant. We have previously done this for postvolcanic stratospheric aerosols [*Russell et al.*, 1993a, 1993b] and for the mineral dust dominated Puerto Rico Dust Experiment (PRIDE) [*Livingston et al.*, 2003] and ACE-Asia [*Schmid et al.*, 2003b; *Redemann et al.*, 2003] campaigns. *Russell et al.* [2004] established correction factors that correlate well with aerosol effective radius and also with Ångström exponent

$$\alpha_\tau(\lambda_1, \lambda_2) = -\ln\left[\tau_p(\lambda_1)/\tau_p(\lambda_2)\right] / \ln(\lambda_1/\lambda_2), \qquad (1)$$

We find the correction factors to be negligible for the Ångström exponents encountered during AIOP.

[20] The total uncertainty $\delta\tau_p(\lambda)$ of the retrieved $\tau_p(\lambda)$, due to uncertainties in calibration, Sun tracking, signal measurement, air mass computation, and corrections of molecular scattering and absorption, was computed following the procedures given by *Russell et al.* [1993a] and *Schmid et al.* [1997]. Note that the impact of tracking errors can be treated as calibration errors taking into account the tracking deviation from the Sun and the measured dependence of each channel's response on this deviation angle. In most instances, $\delta\tau_p(\lambda)$ is dominated by the uncertainty in $V_0(\lambda)$. Neglecting for the moment the dependence of $\delta\tau_p(\lambda)$ on the other factors mentioned above, one obtains [*Russell et al.*, 1993a]

$$\delta\tau_p(\lambda) = \frac{1}{m}\frac{\delta V_0(\lambda)}{V_0(\lambda)} \qquad (2)$$

with

$$m \approx \frac{1}{\cos\theta} \qquad (3)$$

[21] Hence a relative uncertainty of 1% in the calibration constant V_0 will lead to an absolute uncertainty in the

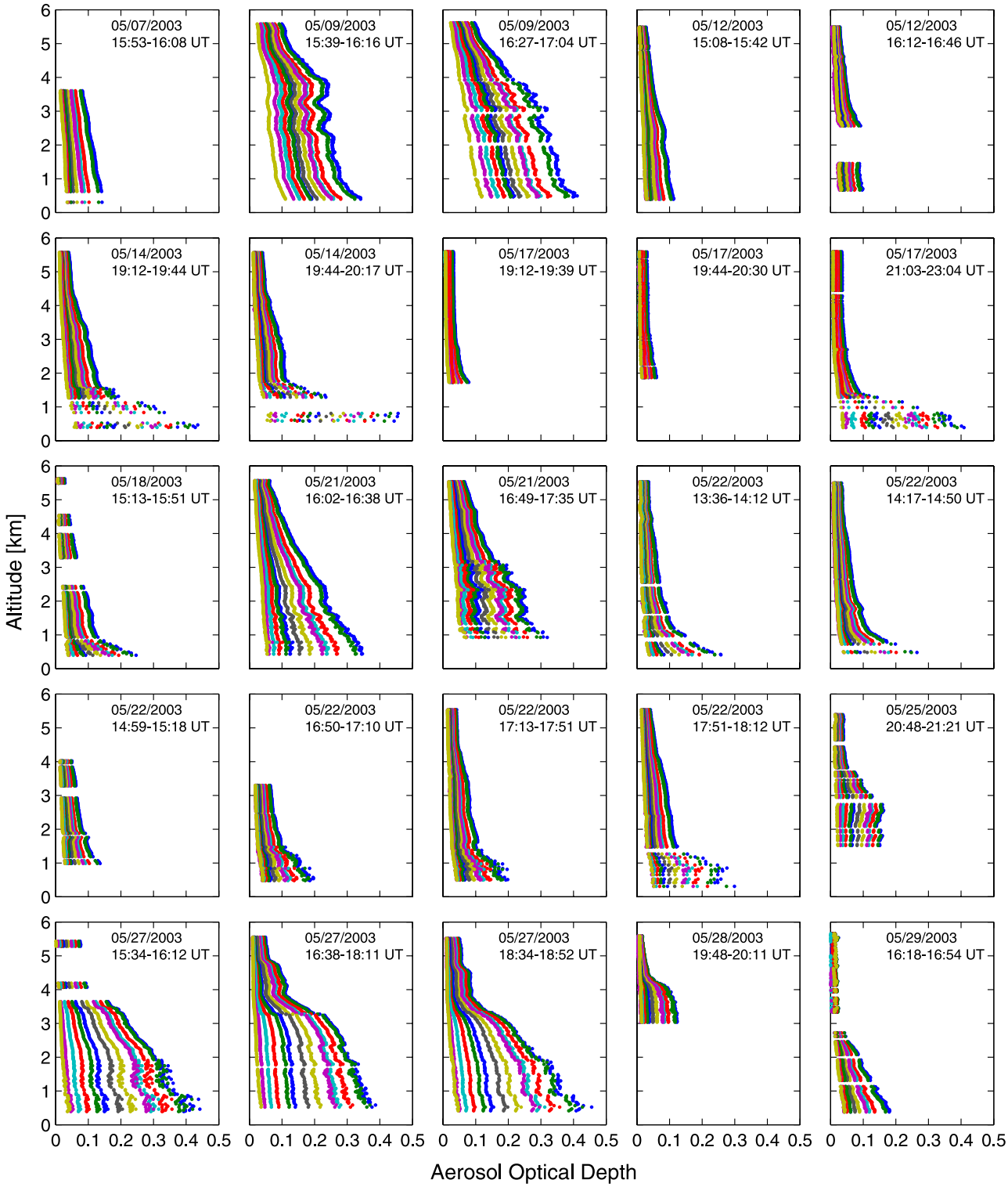

Figure 1. Selection of $\tau_p(\lambda)$ vertical profiles from AIOP.

aerosol optical depth $\delta\tau_p(\lambda)$ of 0.01 for a solar zenith angle $\theta = 0°$ and to smaller uncertainties at larger θ. The $\delta\tau_p(\lambda)$ values obtained using all uncertainties mentioned are part of the archived AATS-14 AIOP data. For the data subset and the wavelengths used most prominently in this study, this resulted in average $\delta\tau_p(\lambda = 453, 519, 675, 1558\ nm) = 0.003, 0.004, 0.005, 0.003$. Note that $\delta\tau_p(\lambda)$ is independent of $\delta\tau_p(\lambda)$ except for diffuse light errors which we neglect for this study [*Russell et al.*, 1993a].

[22] The uncertainty in CWV was computed following *Schmid et al.* [1996]. For the subset used here this resulted in average δCWV = 0.11 g/cm^2.

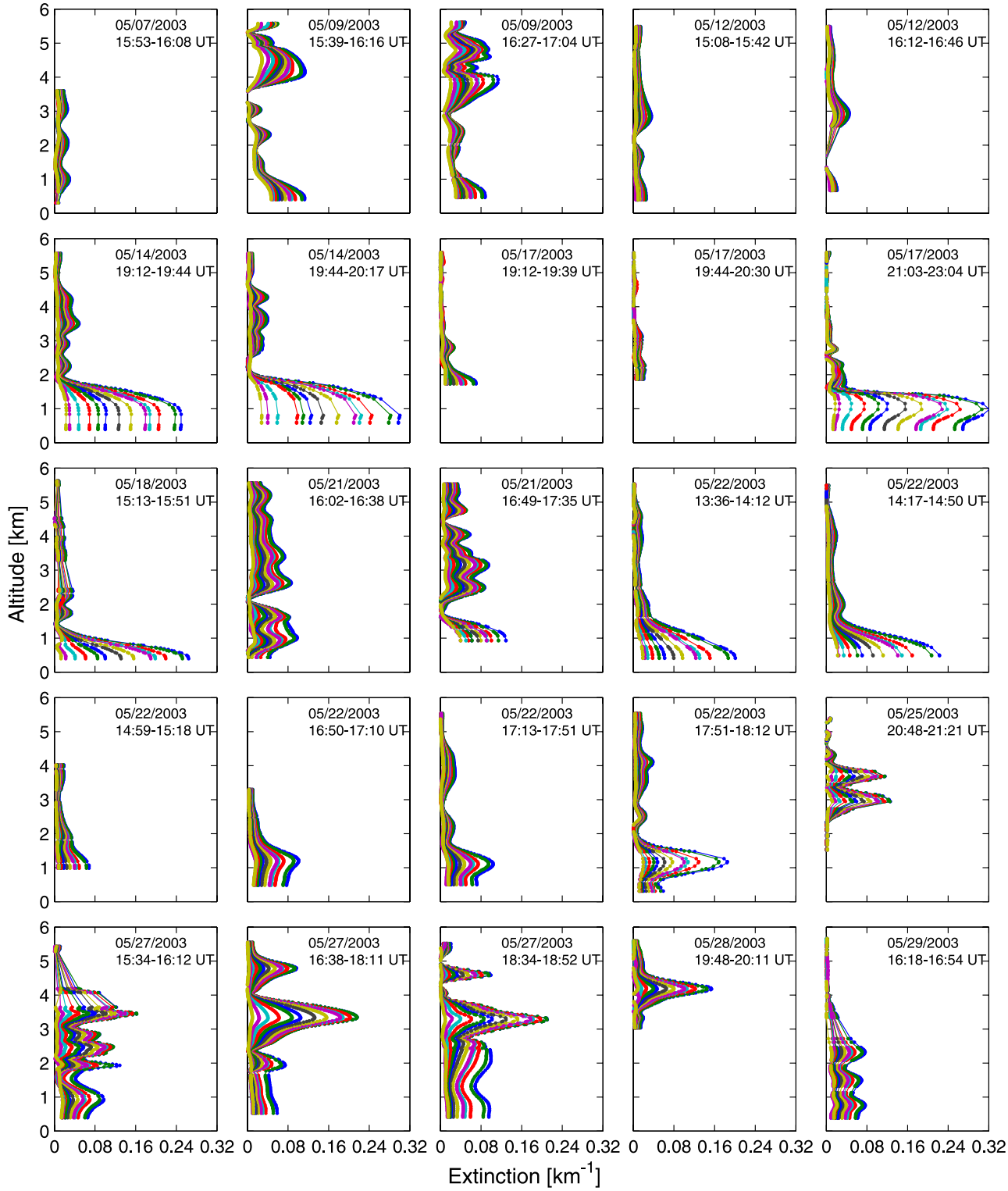

Figure 2. Vertical profiles of $\sigma_{ep}(\lambda)$ derived from the $\tau_p(\lambda)$ profiles shown in Figure 1.

[23] During AIOP the Twin Otter was able to fly as low as 90 m above the land surface, thus allowing measurement of virtually the entire overlying atmospheric column. Flying at different altitudes over a fixed location allows derivation of layer $\tau_p(\lambda)$ and layer water vapor LWV. Differentiation of $\tau_p(\lambda)$ or CWV data obtained in vertical profiles allows derivation of spectral aerosol extinction $\sigma_{ep}(\lambda)$ and water vapor density ρ_w.

[24] During AIOP, AATS-14 measured numerous vertical profiles of $\tau_p(\lambda)$ and CWV. After discarding profiles influenced by considerable spatial inhomogeneity or overlying clouds, we derived spectral aerosol extinction $\sigma_{ep}(\lambda)$ for 26

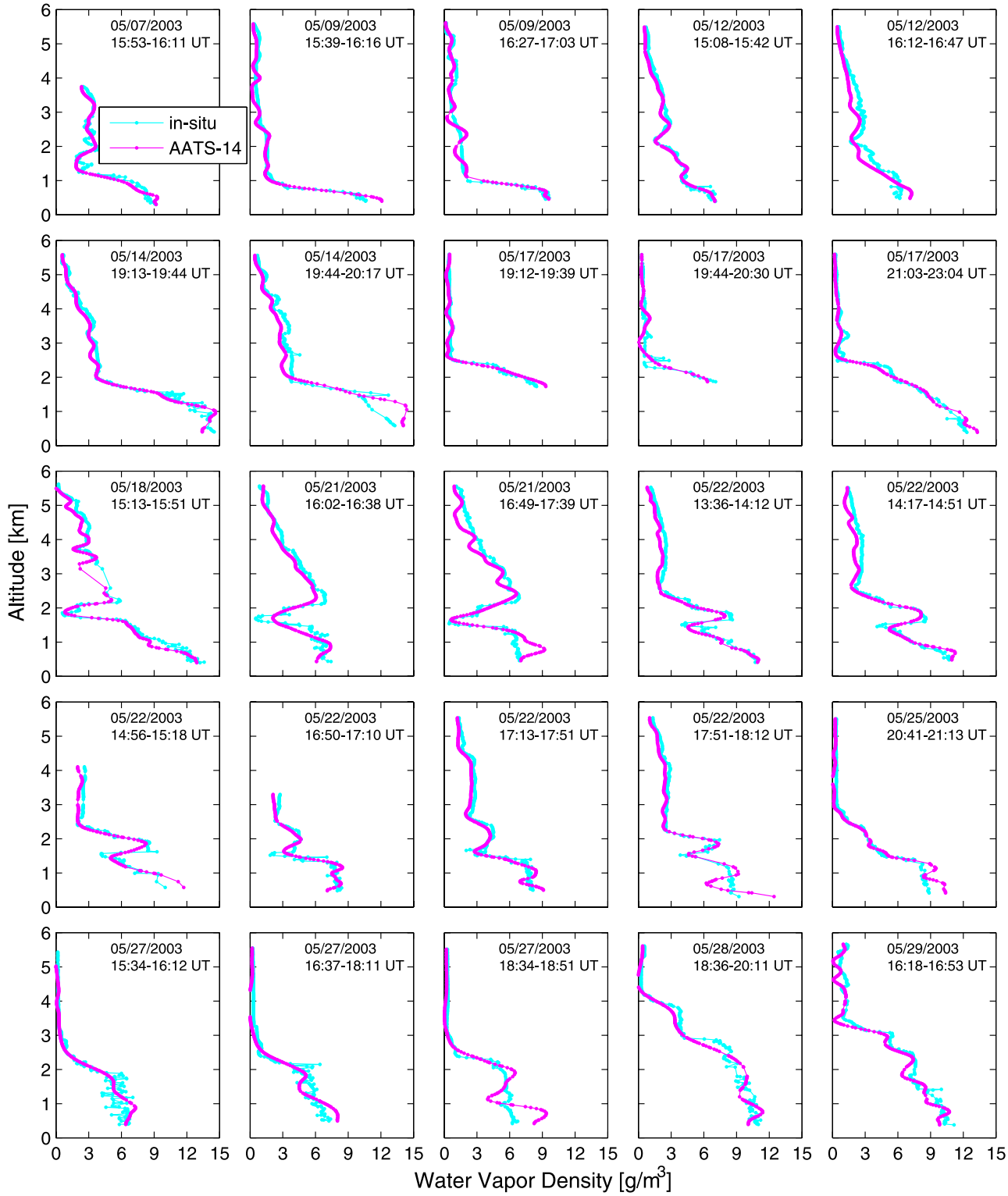

Figure 3. Vertical profiles of ρ_w from AATS-14 and EdgeTech 137-C3 chilled mirror sensor for cases shown in Figure 1.

profiles by differentiating the $\tau_p(\lambda)$ profiles. CWV can be determined despite thin overlying clouds, resulting in 35 CWV and water vapor density (ρ_w) profiles in AIOP. With very few exceptions, the profiles were located directly above the SGP CRF. Figure 1 shows 25 $\tau_p(\lambda)$ vertical profiles. Figure 2 shows the corresponding $\sigma_{ep}(\lambda)$ profiles. The profiles of ρ_w derived from CWV profiles for the same 25 cases are depicted in Figure 3. To facilitate comparisons, we plotted all profiles on the same scale. Gaps in the vertical profiles are caused by temporary blockage of the

direct solar beam by aircraft structures (tail, antennas) or clouds.

[25] Most vertical profiles were acquired within 20 min of flight time. Occasionally, $\tau_p(\lambda)$ or CWV decreased (increased) when the plane descended (ascended). In a horizontally homogeneous, time-invariant atmosphere, this would be impossible. However, in the real atmosphere it can occur because (1) the Sun photometer can only measure the transmittance of the Sun photometer-to-Sun path, (2) that path in general passes through a horizontally inhomogeneous, time-varying atmosphere, and (3) the path and the atmosphere move with respect to each other as the aircraft moves and the wind blows. For the above reasons a point-to-point vertical differentiation of $\tau_p(\lambda)$ or CWV profiles would potentially lead to noisy $\sigma_{ep}(\lambda)$ or ρ_w profiles with large positive and negative excursions. Therefore we average the $\tau_p(\lambda)$ or CWV values over 20-m altitude bins and apply a smoothed spline fit technique prior to vertical differentiation. However, to avoid oversmoothing at altitudes that exhibit actual variations of $\tau_p(\lambda)$ or CWV we occasionally allow $\sigma_{ep}(\lambda)$ or ρ_w to become slightly negative. This can be seen, for example, in Figure 2 (top row, second plot) and Figure 3 (bottom row, fourth plot).

[26] Some of the profiles in Figure 2 show elevated aerosol layers with $\sigma_{ep}(\lambda)$ values exceeding those in the boundary layer. On 9 May 2003, the aerosol in the elevated layers originated from fires in Mexico [*Wang et al.*, 2006]. The elevated layers observed from 25 to 28 May 2003 can be traced back to Siberian fires (P. Colarco et al., unpublished manuscript, 2005). The smoke from the intense 2003 Siberian biomass burning season ultimately traveled around the globe [*Damoah et al.*, 2004].

[27] Because most of the errors in $\tau_p(\lambda)$ or CWV are systematic, they cancel out when differences (such as layer $\tau_p(\lambda)$ or LWV) or differentiations ($\sigma_{ep}(\lambda)$ or ρ_w) are used. However, since the aircraft requires a finite time to fly a vertical profile which has a finite horizontal component, temporal and horizontal variation of the aerosol above the aircraft will lead to uncertainties in the differentiated quantities. The average horizontal variability during AIOP was investigated from $\tau_p(\lambda)$ or CWV measurements during 14 low-level legs. This average variability, together with the vertical and horizontal displacement and the overlying $\tau_p(\lambda)$ found during the vertical profiles, was used to estimate the uncertainties in the differentiated quantities following the formulas in *Redemann et al.* [2003]. This resulted in average $\delta\sigma_{ep}(\lambda = 453, 519, 675, 1558\ nm) = 0.032, 0.029, 0.024, 0.014\ \mathrm{Km}^{-1}$.

2.1.3. Aerosol Extinction From Scattering and Absorption Measurements Aboard the Twin Otter

[28] Light-scattering data were obtained from four integrating nephelometers aboard the Twin Otter. One of these was a three-wavelength (450, 550, 700 nm) integrating nephelometer (model 3563, TSI, St. Paul, Minnesota). The other three were Radiance Research (RR) single-wavelength (540 nm) nephelometers (Model RR903, Radiance Research, Seattle, Washington). All four were calibrated against particle-free air and CO_2 before and at multiple times during the field deployment and were zeroed with particle-free air before each flight.

[29] The TSI nephelometer was operated at a flow rate of 30 l/m and with its inlet heater operational at ~35°C. This resulted in the RH inside the instrument being considerably lower than the ambient RH. The RH inside the TSI nephelometer ranged from near 0 to 35% depending on ambient RH (see Figure 4).

[30] The hygroscopic behavior of the aerosol was determined from the three RR nephelometers operating at different RH. The three RR nephelometers were operated at RHs below ambient, near 85% and at an intermediate level at a flow rate of 6 l/m. The dependence of light-scattering on RH was parameterized by the exponent of equation (4) on the basis of the work of *Kasten* [1969] (see also *Gassó et al.* [2000]).

$$\sigma_{sp}(RH) = \sigma_{sp}(RH_0)f(RH) = \sigma_{sp}(RH_0)\left(\frac{100 - RH}{100 - RH_0}\right)^{-\gamma}. \quad (4)$$

where the zero subscript refers to some low, reference RH, and the exponent, γ, for the measured dependence of light-scattering on RH, is determined by fitting the data to equation (4) as in the work by *Gassó et al.* [2000].

[31] We then utilized γ to correct the low-RH TSI nephelometer scattering signals to the measured ambient RH. Though strictly, the determined γ would apply only to the wavelength of the RR nephelometers (540 nm), we applied it to all three TSI nephelometer wavelengths.

[32] Prior to the humidification correction, the TSI nephelometer $\sigma_{sp}(\lambda)$ values were corrected for angular truncation and non-Lambertian illumination on the basis of the Ångström exponent

$$\alpha_{sp}(\lambda_1, \lambda_2) = -\ln\left[\sigma_{sp}(\lambda_1)/\sigma_{sp}(\lambda_2)\right]/\ln(\lambda_1/\lambda_2), \quad (5)$$

as suggested by *Anderson and Ogren* [1998]. As in the work by *Anderson et al.* [2003], no equivalent correction was done for the RR nephelometers because their truncation parameters and the angular distribution of light inside the instrument have not been determined. However, since the RR nephelometer data are used in a relative sense, i.e., to determine γ, and dominated by submicrometric particles [see *Hallar et al.*, 2006] we expect this to be a small error.

[33] Aerosol light absorption $\sigma_{ap}(\lambda)$ was measured using an improved version of the three-wavelength filter-based Particle/Soot Absorption Photometer (PSAP, λ = 467, 530, 660 nm) described by *Virkkula et al.* [2005]. The data reduction and correction scheme of *Bond et al.* [1999] was applied. Because $\sigma_{ap}(\lambda)$ was measured just downstream of the TSI nephelometer, it was measured under subambient RH (i.e., the same RH as inside the TSI nephelometer to minimize RH-dependent artifacts due to the filter substrate). However, following *Hegg et al.* [1997], no correction was made for the higher RH of the ambient air since experimental data for such a correction are lacking. A study modeling sulfates with black carbon cores by *Redemann et al.* [2001] suggests that absorption humidification factors are negligible for a wide range of atmospheric conditions. However, this may not apply to the considerably more complex real-world aerosol.

[34] The resulting $\sigma_{ap}(\lambda)$ and the nephelometer $\sigma_{sp}(\lambda)$ were adjusted from temperature T_i and pressure p_i inside the

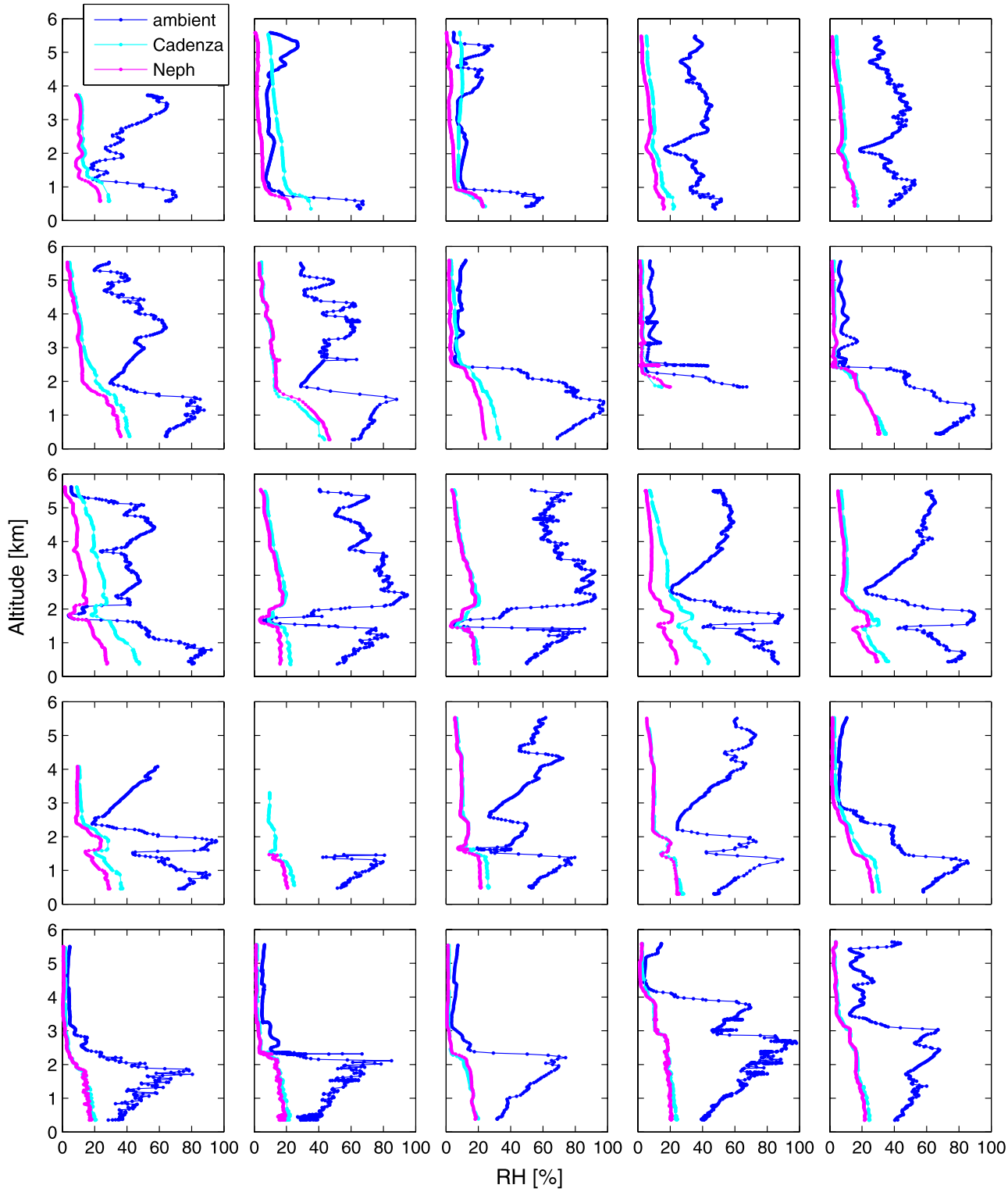

Figure 4. Vertical profiles of ambient RH and RH inside TSI Nephelometer and Cadenza for cases shown in Figures 1–3.

instruments to ambient (outside the aircraft) T_{amb} and p_{amb} by multiplying them with the factor

$$k = \frac{p_{amb}}{p_i} \cdot \frac{T_i}{T_{amb}} \tag{6}$$

Because the cabin of the Twin Otter is not pressurized, p_i is only slightly higher than p_{amb}, however T_i is always larger than T_{amb}.

[35] The reported nephelometer $\sigma_{sp}(\lambda)$ values were adjusted from their blue, green and red center wavelengths

(450, 550, 700 nm) to those of the PSAP instrument (467, 530, 660 nm) using the Ångström relationship in equation (5). For the comparisons shown in this study, the PSAP $\sigma_{ap}(\lambda)$ and nephelometer $\sigma_{sp}(\lambda)$ were adjusted separately (again using an Ångström relationship) to 453, 519 and 675 nm to match AATS-14 and Cadenza (see next section) wavelengths. Aerosol extinction was then calculated as

$$\sigma_{ep}(\lambda) = \sigma_{sp}(\lambda) + \sigma_{ap}(\lambda). \quad (7)$$

[36] In well-controlled laboratory experiments, the uncertainty of Nephelometer-derived $\sigma_{sp}(\lambda)$ when measuring small, dry, laboratory-created particles was found to be 4–7% [*Anderson et al.*, 1996] or as small as 1–2% [*Sheridan et al.*, 2005]. Under such conditions, the uncertainty of PSAP-derived $\sigma_{ap}(\lambda)$ have shown the be as small as 11% [*Sheridan et al.*, 2005]. Airborne measurements of $\sigma_{sp}(\lambda)$ and $\sigma_{ap}(\lambda)$ of atmospheric aerosol at ambient conditions is considerably more complex [i.e., *Anderson et al.*, 2003] and this study attempts to put an upper bound on the resulting uncertainties.

2.1.4. Aerosol Extinction From Cavity Ring-Down Measurements Aboard the Twin Otter

[37] First demonstrated by *O'Keefe and Deacon* [1988], the cavity ring-down (CRD) technique has been used primarily for gaseous absorption spectroscopy (see various papers in the work by *Busch and Busch* [1999]). The use of CRD to measure aerosol extinction is relatively new [*Smith and Atkinson*, 2001; *Strawa et al.*, 2003]. The principle behind CRD can be best described using the so-called 'ping-pong' model. A pulse of laser light is injected into a cavity that consists of two highly reflective mirrors. The mirror reflectivity is typically better than 99.96%. The laser pulse bounces between the two mirrors inside the ring-down cavity like a ping-pong ball. Each time the pulse interacts with the back mirror, a small amount of light (e.g., 0.04%) leaks out. This light is collected and detected with a photomultiplier or similar detector. The intensity of the light leaking out of the back of the ring-down cavity decreases exponentially. It can be shown that the exponential decay, or ring-down time, is related to the mirror reflectivity and the extinction of the material inside the cavity. The extinction coefficient is then obtained by the difference between measurements made when the cell contains filtered air and when the cell contains a particulate-laden flow:

$$\sigma_{ep} = \frac{1}{c}\left(\frac{1}{\kappa_p} - \frac{1}{\kappa_0}\right) \quad (8)$$

where c is the speed of light, and κ_p and κ_0 are the ring-down times of the aerosol laden flow and filtered air, respectively.

[38] Cadenza is the first airborne CRD instrument able to measure aerosol optical properties. The prototype Cadenza instrument as described by *Strawa et al.* [2003] participated successfully in the Reno Aerosol Optics Study (RAOS) [*Sheridan et al.*, 2005]. Cadenza then flew its first and second successful airborne missions in the ADAM and AIOP experiments aboard the CIRPAS Twin Otter. Detailed descriptions of the instrument, the data analysis and comparisons with other methods during AIOP are reported by *Strawa et al.* [2006].

[39] Cadenza operated successfully on all 16 AIOP science flights continuously measuring σ_{ep} at λ = 675 and 1550 nm. Cadenza also measures the aerosol scattering coefficient σ_{sp} at λ = 675 nm. The scattering measurements are discussed by *Hallar et al.* [2006] and *Strawa et al.* [2006]. For 1 min out of every 6 min Cadenza sampled filtered air. The so-derived κ_0 values were then linearly interpolated to the times when particle-laden air was sampled and $\sigma_{ep}(\lambda)$ is determined according to equation (8). While not deliberately heated, the sample air inside Cadenza was nearly at the temperature of the aircraft cabin and consequently drier than the ambient air (see Figure 4). Part of this was caused by ram heating at the aerosol inlet and part was due to heating of the sample line as it carried aerosol from the inlet to the instrument. We then utilized γ along with equation (4) to correct the low-RH Cadenza $\sigma_{ep}(\lambda)$ to outside-the-aircraft RH and also applied the factor in equation (6) to correct to outside-the-aircraft pressure and temperature. Though, strictly, the γ was determined from scattering measurements with the RR nephelometers (λ = 540 nm), we applied it to the Cadenza measurements at λ = 675 nm (σ_{sp} and scattering portion of σ_{ep}) and to σ_{ep}(1550 nm).

[40] In laboratory settings the uncertainty of Cadenza-derived $\sigma_{ep}(\lambda)$ was determined to be 8% [*Sheridan et al.*, 2005] for the prototype instrument and 2% for the flight instrument [*Strawa et al.*, 2006].

2.1.5. Routine Small Aircraft in Situ Measurements

[41] Since March 2000, ARM has been measuring in situ aerosol profiles (IAP) by performing routine flights (2–3 times per week) with a small aircraft (Cessna C-172N) over the SGP site. The aerosol instrument package consists of a three-wavelength TSI nephelometer and a PSAP both measuring at low RH. There is a 1-μm impactor upstream of the aerosol instruments corresponding to a geometric size cut of approximately 0.79 μm (for a particle density of 1.6 g/cm^3). Although the IAP project was not designed to measure ambient $\sigma_{ep}(\lambda)$, *Andrews et al.* [2004] have applied (altitude-independent) corrections for low RH, impactor loss, and limited aircraft ceiling (using information from ground-based nephelometers and Raman lidar) to compare the column-integrated IAP $\sigma_{ep}(\lambda)$ to the $\tau_p(\lambda)$ measured by ground-based Sun photometers. They find the IAP τ_p(550 nm) to have a consistent offset of −0.04.

[42] During AIOP the Cessna flew 14 of its standard flights (i.e., level legs at 9 altitudes between 467 and 3660 m). During five of these flights, the Twin Otter trailed the Cessna on its standard legs. This allowed for detailed interaircraft comparisons which are presented in companion papers by *Hallar et al.* [2006] and *Andrews et al.* [2006].

2.2. Ground-Based Measurements

2.2.1. Sun Photometers

[43] Three ground-based Sun photometers were used to validate AATS-14 $\tau_p(\lambda)$ during low-altitude flybys and to constrain elastic backscatter lidar retrievals. Two of the Sun photometers were AERONET Sun and sky-scanning instruments [*Holben et al.*, 1998, 2001; *Eck et al.*, 1999]. One of the AERONET instruments (98) is a standard Cimel

CE-318 instrument (providing $\tau_p(\lambda)$ at λ = 340, 380, 440, 500, 670, 870 and 1020 nm) that is operated continuously at the SGP CRF. Its data are cloud-screened and quality controlled according to *Smirnov et al.* [2000]. The other AERONET instrument (125), an extended wavelength prototype version with an additional channel at λ = 1640 nm, was deployed specifically for the AIOP. An updated processing scheme was applied to the data from AERONET instrument 125 [*Smirnov*, 2004].

[44] The third Sun photometer was a Normal Incidence Multifilter Radiometer (NIMFR). The instrument consists of a Multifilter Rotating Shadowband Radiometer (MFRSR [*Harrison et al.*, 1994]) "head" to which a collimating tube (FOV 5°) is attached. The NIMFR is mounted on a solar tracker. $\tau_p(\lambda)$ at five wavelengths (λ = 415, 500, 615, 673 and 870 nm) are reported every 20 s. The data set is cloud screened rigorously on the basis of the stability of $\tau_p(\lambda)$ over about a 10-min period using stability limits that were scaled according to the magnitude of $\tau_p(\lambda)$. Expected uncertainties in AOD are ~0.01 for all three Sun photometers.

2.2.2. Micropulse Lidars

[45] The Micropulse Lidar (MPL) [*Spinhirne et al.*, 1995; *Campbell et al.*, 2002] is a single channel (λ = 523 nm), autonomous, eye-safe lidar system originally developed at the NASA Goddard Space Flight Center and now commercially available. One of the MPLs (hereafter referred to as MPLARM) is permanently deployed at the ARM SGP CRF. The second MPL was deployed in support of AIOP as part of the NASA Micropulse Lidar Network (MPLNET) [*Welton et al.*, 2001], a network of ground-based MPL systems colocated with AERONET Sun/sky radiometers.

[46] Vertical profiles of extinction and backscatter were retrieved independently from both colocated MPL systems. The retrieval of independent extinction and backscatter profiles from single-wavelength elastic backscatter lidar (such as an MPL) faces an inherently ill posed problem, in that it requires the extraction of two unknowns (extinction and 180°-backscatter coefficients) from one measurement (the attenuated 180°-backscatter signal) [*Ansmann et al.*, 1990; *Ackermann*, 1998]. However, by assuming a constant value of the extinction-to-backscatter ratio (S_p) throughout an aerosol layer, and by constraining the integrated extinction profile against an independently determined layer $\tau_p(\lambda)$, it is possible to retrieve a unique solution for the extinction and backscatter profiles and calculate a layer-averaged value for S_p [*Welton et al.*, 2000]. This technique yields reasonable results when the atmosphere is well mixed, but may produce overestimates or underestimates of extinction at a given altitude when aerosol properties are highly stratified [*Welton et al.*, 2002].

[47] The retrievals of MPLARM and MPLNET assume an altitude-independent extinction-to-backscatter ratio, S_p. For the total column aerosol optical depth, the MPLARM processing uses cloud-screened $\tau_p(\lambda)$ retrieved from the NIMFR (discussed above), while MPLNET processing uses similarly screened $\tau_p(\lambda)$ [see *Smirnov et al.*, 2000] from the AERONET Sun/sky radiometer located at the ARM SGP CRF (also described above). In as much as the MPL systems, their calibration and constraining $\tau_p(\lambda)$ were completely independent, the retrievals from MPLARM and MPLNET represent independent determinations using fundamentally similar retrieval techniques. An analysis of the AIOP MPLNET results shows an average extinction uncertainty of 7% (not including a possible bias caused by use of a constant S_p value).

2.2.3. Raman Lidar

[48] The CRF Raman lidar (CARL) measures backscattered light at the laser wavelength of 355 nm as well as the water vapor and nitrogen Raman shifted returns, at 408 and 387 nm, respectively. σ_{ep}(355nm) profiles are computed from the derivative of the logarithm of the Raman nitrogen signal with respect to range [*Ansmann et al.*, 1990]. Unlike with elastic backscatter lidars, the Raman technique allows the derivation of σ_{ep} profiles without making an assumption about the profile of the lidar ratio, S_p, and without using the total column τ_p as a constraint [*Ansmann et al.*, 1990; *Ferrare et al.*, 2001].

[49] In April 1997, CARL started to operate at the SGP site as a turnkey, automated system for unattended, around-the-clock profiling of water vapor and aerosols. To facilitate data processing, algorithms were developed to run autonomously delivering water vapor mixing ratio, RH, aerosol scattering ratio, aerosol backscatter coefficient, σ_{ep}, and linear depolarization ratio, as well as integrated values CWV and τ_p [*Turner et al.*, 2001, 2002]. The water vapor measurement performance of CARL has been characterized extensively [see *Ferrare et al.*, 2006, references therein]. However, initial comparisons of τ_p and σ_{ep} have revealed discrepancies among the routine CARL, Sun photometer, and the routine small aircraft in situ measurements described above [*Ferrare et al.*, 2003]. AIOP was conducted in part to resolve these discrepancies. Unfortunately, a gradual loss of the sensitivity of CARL starting about the end of 2001 went unnoticed until after AIOP. In an attempt to reduce or remove these adverse impacts, the automated algorithms were modified and the AIOP data were reprocessed. Major modifications that were made to CARL in 2004 (after AIOP) have dramatically improved the system's sensitivity. The goal is to retrieve σ_{ep} with an uncertainty of 15–20% or 0.025 km^{-1} (whichever is larger). This is discussed in more detail by *Ferrare et al.* [2006].

3. Results

[50] In what follows, we will use the AATS-14 measurement of $\tau_p(\lambda)$ and $\sigma_{ep}(\lambda)$ as a reference against which we will compare all other methods. This choice is driven by the fact that AATS-14 has the largest spectral coverage and can match most of the other instruments' wavelengths relatively closely.

3.1. Comparing $\tau_p(\lambda)$ Obtained From AATS-14 and Ground-Based Sun Photometers

[51] As done in previous airborne campaigns, we assess the in-flight performance of AATS-14 by comparing against surface based Sun photometers. During most of the flights the Twin Otter flew at least one low-altitude leg (~90 m above ground) near the SGP CRF. We compared the AATS-14 $\tau_p(\lambda)$ with those from the AERONET and NIMFR instruments. During 18 such low-altitude flybys the AATS-14 data indicate that the direct beam was not obstructed by clouds. In two cases involving instrument 125, and three cases involving instrument 98, the corresponding

Table 1. Comparison of Airborne and Surface Measured AODs During Low-Altitude Flybys

x		y				lsq Bisector[a]		rms Difference		Bias Difference			
Instrument	λ, nm	Instrument	λ, nm	n	r^2	Slope	Intercept	AOD	%[b]	AOD[c]	%[d]	Mean (x), AOD	Mean (y), AOD
AATS-14	*340*[e]	AERONET 98	340	18	0.933	0.904	0.051	0.035	10%	0.017	5%	0.355	0.372
AATS-14	380	AERONET 98	379	18	0.931	0.919	0.037	0.030	10%	0.012	4%	0.308	0.320
AATS-14	*440*	AERONET 98	440	18	0.924	0.908	0.035	0.029	11%	0.011	4%	0.261	0.272
AATS-14	499	AERONET 98	501	18	0.927	0.904	0.031	0.025	11%	0.008	4%	0.231	0.239
AATS-14	675	AERONET 98	676	18	0.927	0.908	0.015	0.018	11%	0.000	0%	0.159	0.159
AATS-14	*869*	AERONET 98	869	18	0.908	0.890	0.009	0.018	15%	−0.004	−4%	0.124	0.119
AATS-14	1019	AERONET 98	1019	18	0.908	0.893	0.004	0.018	18%	−0.007	−7%	0.102	0.095
AATS-14	*340*	AERONET 125	340	18	0.930	0.930	0.047	0.038	10%	0.023	6%	0.355	0.378
AATS-14	380	AERONET 125	380	18	0.940	0.925	0.046	0.035	11%	0.023	7%	0.308	0.330
AATS-14	440	AERONET 125	440	18	0.942	0.933	0.039	0.032	12%	0.022	8%	0.261	0.282
AATS-14	499	AERONET 125	501	18	0.940	0.933	0.031	0.027	11%	0.016	7%	0.231	0.247
AATS-14	675	AERONET 125	675	18	0.938	0.933	0.019	0.019	11%	0.008	5%	0.159	0.167
AATS-14	*870*	AERONET 125	870	18	0.925	0.940	0.010	0.015	12%	0.002	2%	0.123	0.126
AATS-14	1019	AERONET 125	1020	18	0.922	0.923	0.010	0.015	14%	0.002	2%	0.102	0.104
AATS-14	*1638*	AERONET 125	1638	18	0.921	0.890	0.002	0.014	20%	−0.006	−9%	0.070	0.064
AATS-14	*415*	NIMFR	415	12	0.991	0.953	0.009	0.012	4%	−0.004	−1%	0.284	0.279
AATS-14	499	NIMFR	500	12	0.993	0.968	0.013	0.010	4%	0.006	2%	0.235	0.241
AATS-14	*615*	NIMFR	615	12	0.983	0.955	0.015	0.013	7%	0.007	4%	0.183	0.189
AATS-14	675	NIMFR	673	12	0.993	0.954	0.011	0.008	5%	0.004	2%	0.163	0.167
AATS-14	*870*	NIMFR	870	12	0.993	0.935	0.006	0.007	6%	−0.002	−1%	0.128	0.126

[a]Regression line calculated using linear least squares bisector method [*Sprent and Dolby*, 1980].
[b]Calculated as RMS difference/[0.5·(mean(x) + mean(y)].
[c]Calculated as mean(y-x).
[d]Calculated as mean(y-x)/mean(x).
[e]AOD has been interpolated or extrapolated if wavelength is printed in italics using a quadratic function in ln λ versus ln AOD [see *Schmid et al.*, 2003a].

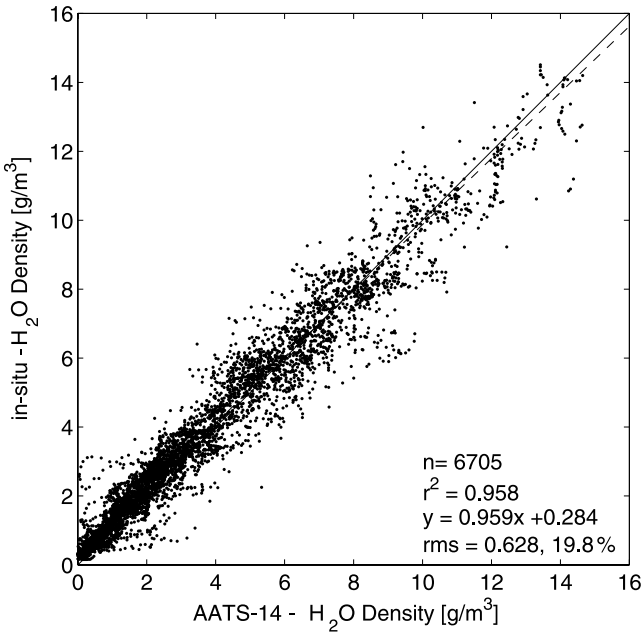

Figure 5. Comparison of ρ_w from AATS-14 and EdgeTech 137-C3 chilled mirror sensor for 35 vertical profiles.

AERONET observations had been screened out in the level 2.0 data. For these cases we reverted to the not-cloud-screened level 1.0 data. It appears that the NIMFR cloud screening is even more conservative, in that only 12 flybys had concurrent NIMFR data. The results of the $\tau_p(\lambda)$ comparison are shown in Table 1.

[52] The agreement between AATS-14 and the AERONET (rms difference = 12%, bias = 2%, averaged over all λ) instruments is similar to what we found from low-altitude flybys over AERONET sites in previous campaigns (i.e., PRIDE [*Livingston et al.*, 2003], SAFARI 2000 [*Schmid et al.*, 2003a], and CLAMS [*Redemann et al.*, 2005]). The agreement between AATS-14 and NIMFR found in AIOP is particularly good (rms difference = 5%, bias = 1%, averaged over all λ), in fact operating four Sun photometers (including AATS-6) side-by-side on the ground in previous ARM IOPs did not result in a higher level of agreement [*Schmid et al.*, 1999].

3.2. Comparison of Water Vapor Profiles

[53] An aircraft in situ measurement of ρ_w is more straightforward than measuring ambient $\sigma_{ep}(\lambda)$. Several redundant sensors aboard the Twin Otter measured static temperature T, static pressure p, and dew point temperature T_d. from which we computed ρ_w using an expression given by *Bögel* [1977].

[54] Since the same vertical differentiation procedure is used to derive $\sigma_{ep}(\lambda)$ and ρ_w from the columnar data $\tau_p(\lambda)$ and CWV, comparing ρ_w obtained from AATS-14 and the aircraft in situ sensors should allow conclusions on the robustness of the AATS-14 differentiated profiles of ρ_w and $\sigma_{ep}(\lambda)$.

[55] In Figure 3, we compare 25 (of 35) vertical profiles of ρ_w derived from AATS-14 and an EdgeTech 137-C3 chilled mirror sensor. We observe excellent correspondence between the two measurements. This also demonstrates that the differentiated column method can successfully reproduce thin (~500 m) dry or humid layers. Figure 5 shows a scatterplot containing all data pairs from all 35 profiles. Figure 6 shows a comparison of the layer water vapor (LWV) amounts. LWV is obtained by integrating the in situ measured ρ_w over the vertical span of the profile and for AATS-14 by subtracting the CWV measured at the top of the profile from CWV measured at the bottom. The complete statistics of the comparison are shown in Table 2. The agreement in this study is better than what we found during ACE-Asia [*Schmid et al.*, 2003b] using the same instrumentation (i.e., in ACE-Asia the RMS difference in ρ_w and LWV was 25% and 17% versus 20% and 7% in AIOP). We attribute this to the fact that the AATS-14 AIOP data were acquired using a different brand 941-nm filter which was delivered with potentially more accurate spectral band pass information.

[56] This study finds the Twin Otter chilled mirror ρ_w to be biased slightly high (5%) with respect to AATS-14. More extensive AIOP water vapor comparisons are discussed in the paper by *Ferrare et al.* [2006].

3.3. Comparison of Aerosol Extinction Profiles

[57] For the extinction comparison, the profiles from the six methods were binned in 20-m altitude bins between 0 and 8 km above sea level. Naturally, empty bins were excluded from the comparisons. In virtually all of the comparisons the AATS-14 values were used as the independent variable x, however the linear regressions were established using the linear least squares bisector (lsq-bs) method which minimizes the quadratic distances to the regression line in x and y directions [*Sprent and Dolby*, 1980].

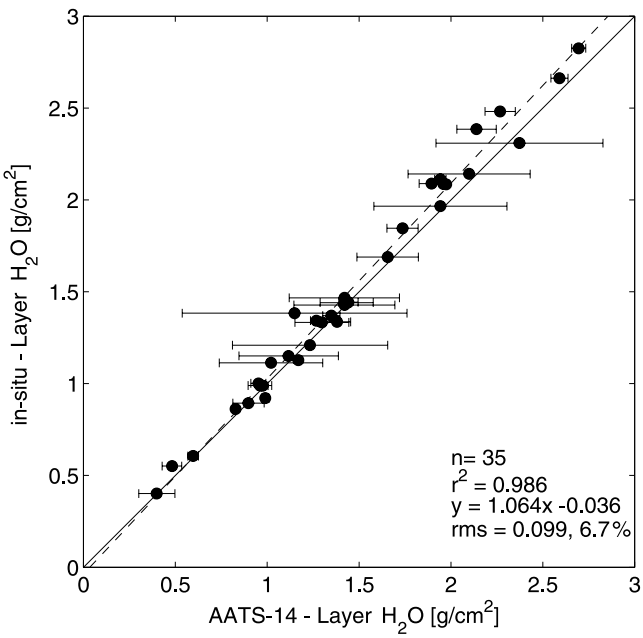

Figure 6. Comparison of LWV from AATS-14 and EdgeTech 137-C3 chilled mirror sensor for 35 vertical profiles. AATS-14 error bars are based on horizontal distance spanned by a profile, combined with average horizontal variability of CWV in AIOP flights.

Table 2. Comparison of Water Vapor Retrieved From AATS-14 and EdgeTech 137-C3 Chilled Mirror[a]

x		y				lsq Bisector		rms Difference		Bias Difference			
Instrument	Quantity	Instrument	Quantity	n	r^2	Slope	Intercept	g/cm^2	%	g/cm^2	%	Mean (x), g/cm^2	Mean (y), g/cm^2
AATS-14	layer H_2O	chilled mirror	layer H_2O	35	0.986	1.064	−0.036	0.099	7%	0.057	4%	1.459	1.515
AATS-14	H_2O dens.	chilled mirror	H_2O dens.	6705	0.958	0.959	0.284	0.628[b]	20%	0.157[b]	5%	3.088[b]	3.245[b]

[a]Footnotes in Table 1 detail how statistical results were calculated.
[b]Unit is g/m^3.

[58] The Nephelometer+PSAP extinctions were adjusted to the closest AATS-14 wavelengths. In contrast, the CARL, MPL and Cadenza instruments' wavelengths are matched closely enough by an AATS-14 wavelength that no further adjustment is required. This resulted in eight comparisons between AATS-14 and the other five methods at five different wavelengths (see Table 3).

[59] Plotting the profiles allows a visual evaluation on a profile-by-profile basis. Figure 7 makes such a comparison for σ_{ep}(675nm) from AATS-14 and Nephelometer+PSAP. In this representation, the Cadenza σ_{ep}(675nm) profiles are virtually indistinguishable from Nephelometer+PSAP data points and are therefore not plotted in Figure 7. The high correlation (r^2 = 0.963) between the two in situ measurements is evident in the scatterplot representation in Figure 8. Averaged over all profiles, the Cadenza σ_{ep}(675nm) are higher by 4.7% (on the basis of lsq-bs regression line slope) or 6.5% (on the basis of bias) than the Nephelometer+PSAP values. This result and those presented by *Strawa et al.* [2006] represent a very successful demonstration of the airborne application of the CRD method to measure $\sigma_{ep}(\lambda)$.

[60] Figure 7 shows cases where AATS-14 σ_{ep}(675 nm) are in good agreement with the in situ measurements, cases where the AATS-14 values oscillate around the in situ data and cases where the AATS-14 values are higher. As an illustration, the scatterplot in Figure 9 shows that Cadenza σ_{ep}(675 nm) are 11% (on the basis of lsq-bs slope) to 13% (bias) lower than the AATS-14 values. Figure 9 shows considerably more scatter than the comparison of the two in situ instruments in Figure 8. This is a result of (1) two very different sampling strategies in a nonhomogenous aerosol field and (2) real differences between the AATS-14 and in situ measurements.

[61] An alternative way of assessing potential biases in extinction profiles lies in comparing layer $\tau_p(\lambda)$. Layer $\tau_p(\lambda)$ is obtained by integrating the in situ or lidar measured $\sigma_{ep}(\lambda)$ over the vertical span of the AATS-14 profile and for AATS-14 by subtracting the $\tau_p(\lambda)$ measured at the top from the $\tau_p(\lambda)$ measured at the bottom of the profile. As an example, the scatterplot in Figure 10 shows that Cadenza layer τ_p(675 nm) are lower by 15% (on the basis of lsq-bs slope) to 16% (bias) than the AATS-14 values. The layer $\tau_p(\lambda)$ comparisons from all methods are summarized in Table 4.

[62] The comparisons in Tables 3 and 4 show that the in situ methods yield consistently lower $\sigma_{ep}(\lambda)$ and layer $\tau_p(\lambda)$ than AATS-14. All regression lines exhibit slopes smaller than 1 with very small intercepts indicating a proportional difference rather than a systematic offset. On the basis of the slopes, we find the Nephelometer+PSAP $\sigma_{ep}(\lambda)$ to be lower by 7%, 10% and 14% (λ = 453, 519, 675 nm). The Cadenza $\sigma_{ep}(\lambda)$ are lower by 11% (λ = 675 nm) and 40% (λ = 1550 nm). These slopes, the slopes in the layer AOD comparison and also the relative biases in $\sigma_{ep}(\lambda)$ and layer $\tau_p(\lambda)$ show a distinct wavelength dependence: The low bias of the in situ measurement with respect to AATS-14 increases with increasing wavelength. Partial loss of larger particles during sampling would cause the observed spectral behavior. However, so far we have not considered a potential wavelength dependence of the humidification correction in equation (4). Indeed, a 1-year analysis (March 2000 to February 2001) of surface-based dry and humidified

Table 3. Comparison of Aerosol Extinction Vertical Profiles From Six Different Methods[a]

x		y				lsq Bisector		rms Difference		Bias Difference			
Instrument	λ, nm	Instrument	λ, nm	n	r^2	Slope	Intercept	km^{-1}	%	km^{-1}	%	Mean (x), km^{-1}	Mean (y), km^{-1}
AATS-14	354	Raman	355	468	0.663	1.080	0.024	0.050	73%	0.029	54%	0.053	0.082
AATS-14	453	Neph+PSAP	453	3493	0.725	0.931	−0.002	0.019	67%	−0.004	−13%	0.031	0.027
AATS-14	519	Neph+PSAP	519	3493	0.714	0.900	−0.001	0.017	70%	−0.004	−15%	0.026	0.023
AATS-14	519	MPLNET	523	587	0.529	0.961	0.005	0.023	72%	0.004	13%	0.030	0.034
AATS-14	519	MPLARM	523	2073	0.447	0.879	0.011	0.026	78%	0.007	24%	0.030	0.037
AATS-14	675	Neph+PSAP	675	3493	0.693	0.860	−0.001	0.013	74%	−0.003	−17%	0.019	0.016
AATS-14	675	Cadenza	675	2914	0.711	0.893	−0.000	0.013	71%	−0.002	−13%	0.019	0.016
AATS-14	1558	Cadenza	1550	2914	0.627	0.602	0.000	0.006	98%	−0.004	−45%	0.008	0.005
Neph+PSAP	675	Cadenza	675	3772	0.964	1.047	0.000	0.005	25%	0.001	7%	0.017	0.018

[a]Footnotes in Table 1 detail how statistical results were calculated.

$\sigma_{sp}(\lambda$ = 450, 550, 700 nm) (submicron particles only) measured with a TSI nephelometer at the SGP CRF [*Sheridan et al.*, 2001], shows a distinct wavelength dependence [*Sivaraman et al.*, 2004] of γ (see Table 5). This implies that the humidification correction should increase from blue to green and red (and potentially to the near infrared). *Kotchenruther et al.* [1999] determined a similar wavelength dependence of the humidification factor from airborne measurements during TARFOX. Hence part of the spectral behavior of the low bias observed in this study could stem from a not entirely adequate humidification correction.

[63] To test the hypothesis that the low bias is caused by sampling losses of larger particles or an insufficient humidification correction, we stratified the extinction comparison by ambient RH and by α_{ep} from AATS-14 (a proxy for particle size). As shown in Table 6, the low bias decreases significantly with decreasing ambient RH for both Neph+PSAP and Cadenza. The effect is smallest for the 1550-nm Cadenza wavelength. The low bias of Neph+PSAP $\sigma_{ep}(\lambda)$ seems to be poorly correlated to particle size based on α_{ep} whereas the low bias of Cadenza $\sigma_{ep}(\lambda)$ is smaller for larger α_{ep} values (i.e., smaller particle sizes). Hence the sensitivity of the low bias to ambient RH seems obvious for Neph+PSAP and Cadenza whereas its sensitivity to α_{ep} is obvious only in the Cadenza data.

[64] Subsequently we further investigated the applied humidity correction (equation (4)). For the 26 vertical profiles we find a median value of γ = 0.30 leading to median f(RH) values of 1.13 and 1.14 for Cadenza and TSI Nephelometer, respectively. We find that in ~20% of all cases a determination of γ from the RR Nephelometers was not possible and γ was set to 0 (i.e., f(RH) = 1). Because most of these cases are associated with very low ambient RH, assuming γ = 0.30 (the median value) instead of γ = 0, reduced the low biases only by about 0.5%. *Ferrare et al.* [2006] suggest that the Twin Otter ambient RH measurements are ~3% low. Increasing ambient RH by that amount decreases the low bias by another 2–3%. We then determined the factors by which γ needed to be increased further to eliminate the remaining biases. While the resulting factors (Table 5) are relatively large, 1.44 to 1.7, the resulting median values for γ are fairly close to the 1-year ground-based average found by *Sivaraman et al.* [2004]. It is important to note that the increased values for γ did not decrease the r^2 values of the $\sigma_{ep}(\lambda)$ comparisons except for the 1550-nm Cadenza wavelength, where obviously the low bias cannot be eliminated with an increased f(RH) correction alone.

[65] Lidar data concurrent with a Twin Otter vertical profile were available in 11 (CARL), 13 (MPLNET) and 19 (MPLARM) cases. Comparison of CARL data with AATS-14 and in situ data is discussed in detail in a companion paper [*Ferrare et al.*, 2006]. As summarized in Tables 3 and 4, CARL σ_{ep}(355 nm) and layer τ_p(355 nm) are significantly higher than the AATS-14 values. The lsq-bs regression line between AATS-14 and CARL σ_{ep}(355 nm) reveals an intercept of 0.024 Km^{-1} indicating a systematic offset. The mean difference between the two data sets is 0.029 Km^{-1} or 54% for the average σ_{ep}(354 nm) of 0.053 Km^{-1}. We believe that this high bias was primarily due to the unnoticed loss of sensitivity of CARL leading up

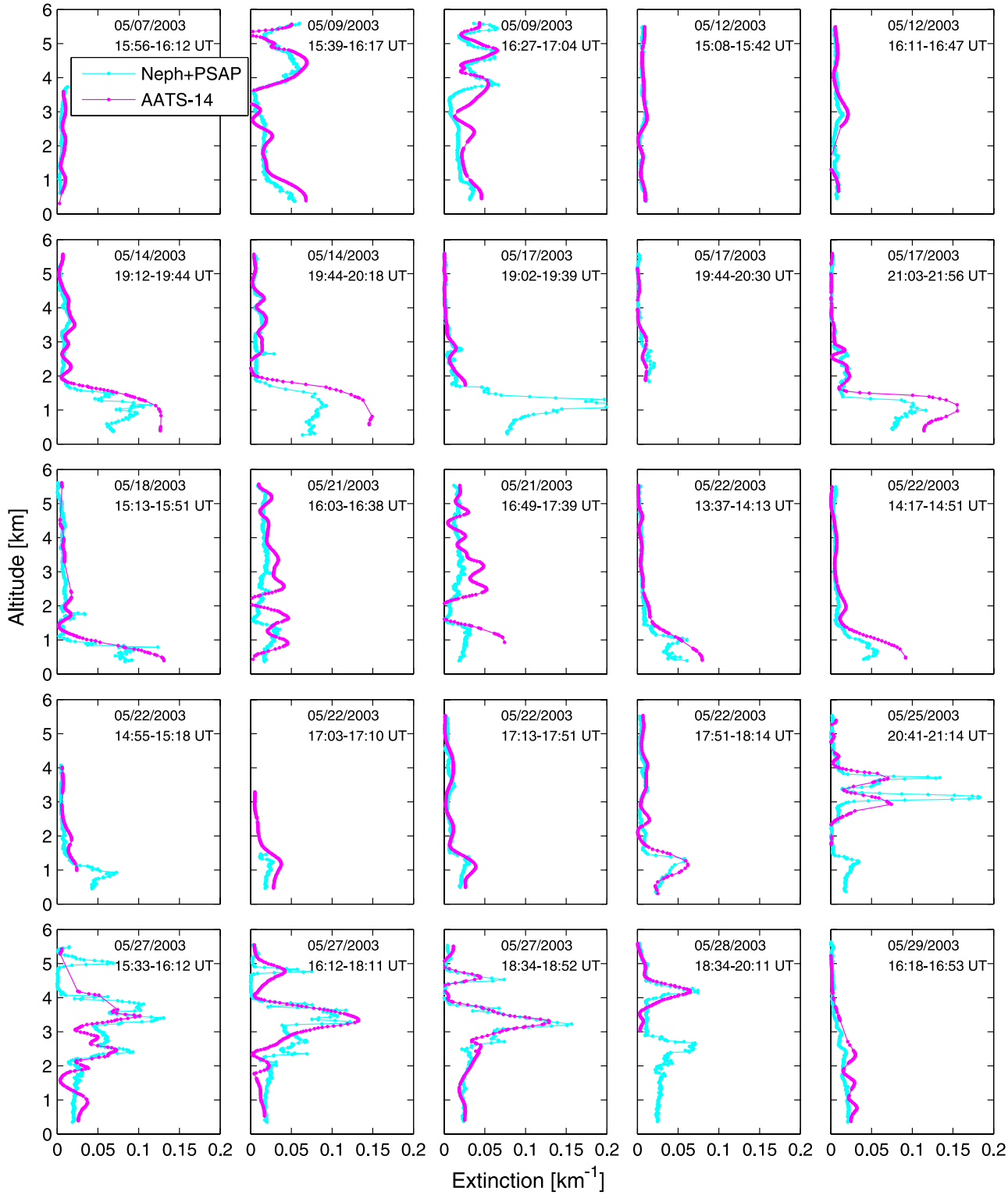

Figure 7. Vertical profiles of σ_{ep}(675 nm) from Nephelometer+PSAP and AATS-14 for the cases shown in Figure 2. (The Cadenza σ_{ep}(675nm) profiles are virtually indistinguishable from Nephelometer+PSAP data points and are therefore not plotted.)

to AIOP; this reduction in sensitivity led to increased calibration errors, larger random errors, and greater uncertainties in maintaining proper alignment, all of which contributed to these differences. We expect better agreement in future comparisons from the recently upgraded CARL system.

[66] Figure 11 shows vertical profiles of σ_{ep} from Nephelometer+PSAP and the two Micro Pulse Lidars. The three

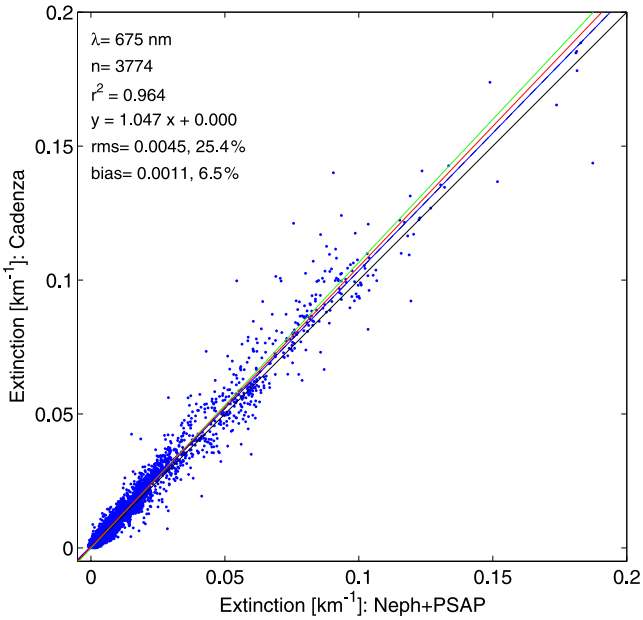

Figure 8. Comparison of σ_{ep}(675 nm) from Nephelometer+PSAP and Cadenza for all 26 vertical profiles. Black indicates 1:1 line, blue indicates regular y versus x regression, green indicates inverted x versus y regression, and red indicates bisector of blue and green lines (i.e., least squares bisector method [*Sprent and Dolby*, 1980]).

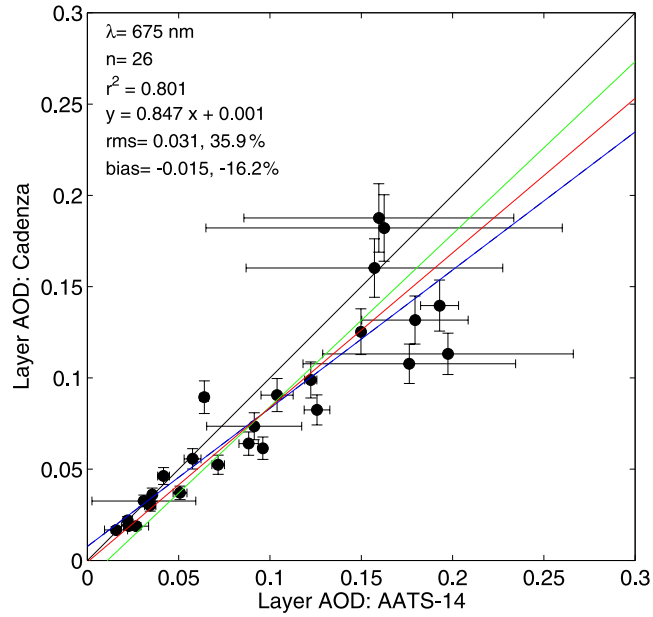

Figure 10. Comparison of layer τ_p(675 nm) from AATS-14 and Cadenza for all 26 vertical profiles. Regression lines are as in Figure 8. AATS-14 error bars are based on horizontal distance spanned by a profile, combined with average horizontal variability of AOD in AIOP flights. Cadenza error bars reflect 10% uncertainty.

data sets show good agreement for the vertical distribution of aerosol layers including fairly thin layers. However, the absolute magnitudes of σ_{ep}(519/523 nm) differ. As shown by Table 3, the lsq-bs regression lines of σ_{ep}(523 nm) of MPLNET versus AATS-14 and MPLARM versus AATS-14 reveal intercepts of 0.005 and 0.011 Km^{-1} revealing systematic high biases. The bias difference is 0.004 Km^{-1} (13%) between AATS-14 and MPLNET and 0.007 Km^{-1} (24%) between AATS-14 and MPLARM for the average σ_{ep}(519 nm) of 0.030 Km^{-1}. Surprisingly, the layer τ_p(519/523 nm) comparisons (Table 4) show high biases with respect to AATS-14 of 0.023 (MPLNET) and 0.025 (MPLARM) that exceed the biases between AATS-14 and AERONET 98 (0.008) and NIMFR (0.006) to which the MPL retrievals are anchored. Figure 12 shows the cumulative integrals (top to bottom) of the MPL σ_{ep}(523 nm) which is equivalent to a τ_p profile as measured by AATS-14. We find that the cumulative integral of MPLNET and MPLARM σ_{ep}(523 nm) at the top of the AATS-14 profile average 0.014 lower than the AATS-14 τ_p(519 nm). This discrepancy is likely caused by the fact that the MPL retrievals determine a maximum layer height z_{max} (typically below 8–10 km) above which σ_{ep}(523 nm) is set to 0. The retrievals then assume that the integrated extinction between the surface and z_{max} make up the total column τ_p(523 nm) to which they are anchored. Neglecting the cumulative σ_{ep}(523 nm) from top-of-the-atmosphere to z_{max} will therefore introduce a slight high bias in the MPLNET σ_{ep}(523 nm) and layer τ_p(523 nm) retrievals. Figure 12 shows that, apart from the small bias discussed above, the τ_p profiles start out at similar values at the top of the AATS-14 profiles and end at similar values at the bottom because of the MPL retrievals' anchoring. In between there are discrepancies, though, indicating that the σ_{ep} are distributed differently over the vertical profile. This is apparent in Figure 11 where, compared to Nephelometer +PSAP σ_{ep}(523 nm), MPLARM indicates lower σ_{ep}(523 nm) in elevated layers above 3 km, but higher values below 2 km. This may be an effect of the MPL retrievals assuming that S_p

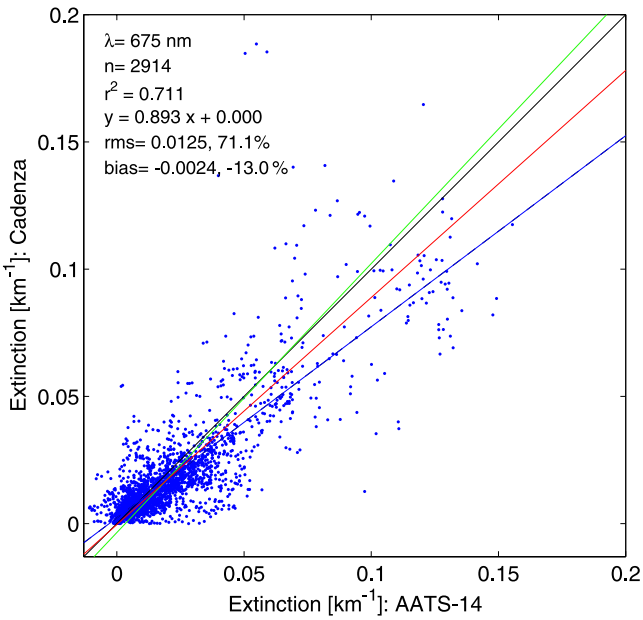

Figure 9. Comparison of σ_{ep}(675 nm) from AATS-14 and Cadenza for all 26 vertical profiles. Regression lines are as in Figure 8.

Table 4. Comparison of Layer $\tau_p(\lambda)$ From Six Different Methods[a]

x		y				lsq Bisector		rms Difference		Bias Difference			
Instrument	λ, nm	Instrument	λ, nm	n	r^2	Slope	Intercept	AOD	%	AOD	%	Mean (x), AOD	Mean (y), AOD
AATS-14	354	Raman	354	11	0.834	1.510	0.005	0.106	55%	0.083	55%	0.152	0.235
AATS-14	453	Neph+PSAP	453	26	0.834	0.879	−0.006	0.047	33%	−0.025	−16%	0.158	0.133
AATS-14	519	Neph+PSAP	519	26	0.824	0.855	−0.005	0.044	36%	−0.024	−18%	0.134	0.110
AATS-14	519	MPLNET	523	13	0.946	0.995	0.024	0.030	18%	0.023	15%	0.157	0.181
AATS-14	519	MPLARM	523	19	0.966	1.055	0.017	0.031	19%	0.025	17%	0.151	0.177
AATS-14	675	Neph+PSAP	675	26	0.822	0.826	−0.003	0.033	39%	−0.020	−21%	0.094	0.075
AATS-14	675	Cadenza	675	26	0.802	0.847	−0.001	0.031	36%	−0.015	−16%	0.095	0.080
AATS-14	1558	Cadenza	1550	26	0.885	0.564	−0.001	0.022	75%	−0.017	−45%	0.037	0.020

[a]Footnotes in Table 1 detail how statistical results were calculated.

Table 5. Comparison of Exponent γ in Humidification Correction

Wavelength	γ Used[a]	Ratio	γ Neph[b]	Ratio	γ Cadenza[b]	γ Ground[c]
Blue	0.30	1.44	0.43			0.39
Green	0.30	1.55	0.47			0.44
Red	0.30	1.70	0.51	1.48	0.44	0.49

[a]Median value used in this study; derived from airborne RR Nephelometers.

[b]Median value needed to eliminate bias in $\sigma_{ep}(\lambda)$ with respect to AATS-14.

[c]Median value from 1-year analysis (March 2000 to February 2001) of surface-based dry and humidified σ_{sp} submicron particles only) measured with a TSI nephelometer at the SGP CRF [*Sivaraman et al.*, 2004].

is altitude-independent and/or due to inadequate corrections for overlap or afterpulse.

4. Results From Previous Campaigns

4.1. Aerosol Extinction From Scattering and Absorption Measurements

[67] In numerous field campaigns since 1996 we have compared $\sigma_{ep}(\lambda)$ and layer $\tau_p(\lambda)$ obtained from Nephelometer+PSAP measurements with either AATS-6 or -14. As shown in Table 7, seven data sets from six field campaigns were reported in eight studies. The data sets were obtained aboard five different airplanes. Different metrics have been used in the eight studies to describe the level of agreement making direct comparisons difficult. For each study we have recomputed the coefficient of determination, r^2, and the relative bias differences in layer $\tau_p(\lambda)$. The studies cover wavelengths between 450 and 700 nm. We find that with respect to AATS-14 (or -6) the layer $\tau_p(\lambda)$ value from Nephelometer+PSAP are biased low by −4 to −33%. The average low bias (all λ) is −17%.

[68] Several studies have compared column integrated $\sigma_{ep}(\lambda)$ with ground-based Sun photometer measurements of $\tau_p(\lambda)$ [*Remer et al.*, 1997; *Kato et al.*, 2000; *Andrews et al.*, 2004]. Invariably they find the in situ derived $\tau_p(\lambda)$ to be biased low with respect to the Sun photometer measurements. However, in all three studies assumptions about the aerosol above the maximum aircraft sampling altitude had to be made, humidification factors were not measured on the aircraft, and aircraft inlets were not suitable for sampling of larger aerosol particles.

4.2. Extinction Calculated From Airborne Particle Size Distributions

[69] In three campaigns since 1996 we have compared $\sigma_{ep}(\lambda)$ and layer $\tau_p(\lambda)$ calculated from airborne measurements of particle size distributions with either AATS-6 or -14. As shown in Table 8, excellent agreement was achieved in ACE-2 and ACE-Asia but poorer agreement resulted from the TARFOX data set. While there is also a tendency for the $\sigma_{ep}(\lambda)$ and layer $\tau_p(\lambda)$ calculated from in situ data to be lower than the AATS-14 values, we observe the low bias found in ACE-2 and ACE-Asia to be smaller than in the corresponding Nephelometer+PSAP comparisons listed in Table 7. However, the reverse is the case for the TARFOX data set.

[70] To our knowledge, *Clarke et al.* [1996] present the only other study where layer $\tau_p(\lambda)$ calculated from particle size distributions were compared to the values obtained with

Table 6. Bias Differences in $\sigma_{ep}(\lambda)$ With Respect to AATS-14 as a Function of Ambient RH and α_{ep}

		RH_{amb}, %				α_{vis}			
Instrument	Wavelength, nm	0–100	0–33	33–66	66–100	0–2.5	0–1	1–1.5	1.5–2.5
Neph+PSAP	453	−13%	−2%	−16%	−26%	−15%	−17%	−13%	−19%
Neph+PSAP	519	−15%	−4%	−17%	−29%	−18%	−20%	−16%	−20%
Neph+PSAP	675	−17%	−8%	−18%	−34%	−21%	−25%	−19%	−19%
Cadenza	675	−13%	−8%	−11%	−23%	−17%	−28%	−15%	−10%
		RH_{amb}, %				α_{NIR}			
Instrument	Wavelength, nm	0–100	0–33	33–66	66–100	−0.5–2.5	−0.5–0.5	0.5–1	1–2.5
Cadenza	1550	−45%	−40%	−48%	−49%	−47%	−53%	−49%	−40%

an airborne Sun photometer (different from AATS). Good agreement was achieved for a profile dominated by pollutant aerosol but the calculated σ_{ep}(550 nm) values were 50% lower in a profile featuring an elevated Saharan dust layer.

4.3. Extinction From Surface-Based and Airborne Lidars

[71] In numerous campaigns we have compared $\sigma_{ep}(\lambda)$ and $\tau_p(\lambda)$ vertical profiles from one of the AATS instruments with surface-based or airborne lidars (see Table 9). The results involving seven different types of lidar systems have been published in 10 studies. Unfortunately we found it difficult to convert the results from all 10 studies into one quantitative metric. Therefore we use qualitative terms to describe the bias differences in $\sigma_{ep}(\lambda)$. As can be seen from Table 9, many comparisons result in small or no biases, however the biases that do occur are positive (i.e., lidar $\sigma_{ep}(\lambda)$ larger than AATS values).

[72] *Masonis et al.* [2002] compared aircraft in situ and Raman lidar profiles of σ_{ep} and 180° backscattering during the 1999 Indian Ocean Experiment (INDOEX). They found the lidar-derived values to be ~30% larger than the in situ–derived values. *Petzold et al.* [2002] report agreement within 30% (rms) for 180° backscattering measured with a six-wavelength Raman/Mie lidar and calculated from airborne size distribution measurements during the Lindenberg Aerosol Characterization Experiment (LACE 98).

5. Summary and Conclusions

[73] AIOP yielded one of the best measurement sets obtained to date to assess our ability to measure the vertical profile of ambient aerosol extinction $\sigma_{ep}(\lambda)$. Extensive vertical profiling of the CIRPAS Twin Otter, carrying state-of-the-art aerosol and radiation instrumentation, over the heavily instrumented ARM CRF allowed us to compare 11 to 26 $\sigma_{ep}(\lambda)$ profiles obtained from 6 different instruments: airborne Sun photometer (AATS-14), airborne nephelometer plus absorption photometer (Nephelometer+PSAP), airborne cavity ring-down system (Cadenza), ground-based Raman lidar (CARL) and 2 ground-based elastic backscatter lidars (MPLARM and MPLNET).

[74] We find good agreement among the in situ measurements, Cadenza and Nephelometer+PSAP, on the Twin Otter aircraft. Averaged over 25 profiles, the Cadenza σ_{ep}(675nm) are higher by 6.5% (bias difference) than the Nephelometer+PSAP values. This represents a very successful demonstration of the first airborne application of the cavity ring-down method to measure $\sigma_{ep}(\lambda)$.

[75] Subsequently we used the AATS-14 measurement of $\tau_p(\lambda)$ and $\sigma_{ep}(\lambda)$ as a reference against which we compared all other methods. This choice was driven by the fact that AATS-14 has the largest spectral coverage and can match most of the other instruments' wavelengths relatively closely.

[76] When compared to AATS-14 $\sigma_{ep}(\lambda)$, we find the in situ measurements to be biased low (0.002–0.004 Km^{-1} equivalent to 13–17% in the visible, or 44% in the near-infrared). The low bias is also apparent when considering layer $\tau_p(\lambda)$. The statistical quantities we investigated show that the differences (which should be considered modest, at least for the visible) are proportional differences rather than systematic offsets. We also find the low bias to increase with increasing wavelength.

[77] On the other hand, we find that with respect to AATS-14, the $\sigma_{ep}(\lambda)$ values from all 3 lidars are biased high: Bias differences are 0.004 Km^{-1} (13%) and 0.007 Km^{-1} (24%) for the two elastic backscatter lidars (MPLNET and MPLARM, λ = 523 nm) and 0.029 Km^{-1} (54%) for the Raman lidar (λ = 355 nm). Unlike the differences found between AATS-14 and the in situ measurements, the differences between AATS-14 and the three lidars have the nature of an offset. This causes the relative bias to decrease at larger $\sigma_{ep}(\lambda)$ (i.e., bias between AATS and CARL reduces to 10% if only σ_{ep}(355 nm) > 0.15 Km^{-1} are considered [*Ferrare et al.*, 2006]). An unnoticed loss of sensitivity of the Raman lidar had occurred leading up to AIOP, and we expect better agreement from the recently restored system. However, the present comparison between AATS-14 and CARL is valuable as it assesses the daytime retrievals of σ_{ep}(355 nm) of a Raman lidar in an operational setting. CARL is the only Raman lidar in the world designed to autonomously provide a continuous day and nighttime 10-year data record [*Turner et al.*, 2002].

[78] We emphasize the assessment of the uncertainties in the AATS-14 retrieved quantities. The instrument was calibrated at the Mauna Loa Observatory (MLO), Hawaii, 1.5 months before and 1.5 months after the AIOP campaign and the calibration constants were fine tuned within the bounds of premission and postmission calibration by inspecting low-$\tau_p(\lambda)$ spectra obtained near maximum flight altitude (5.6 km).

[79] The in-flight performance of AATS-14 was assessed by comparing $\tau_p(\lambda)$ obtained during low-level legs (~90 m) against ground-based Sun photometers. The agreement between AATS-14 and two AERONET Sun photometers (rms difference = 12%, bias = 2%, averaged over all λ) is

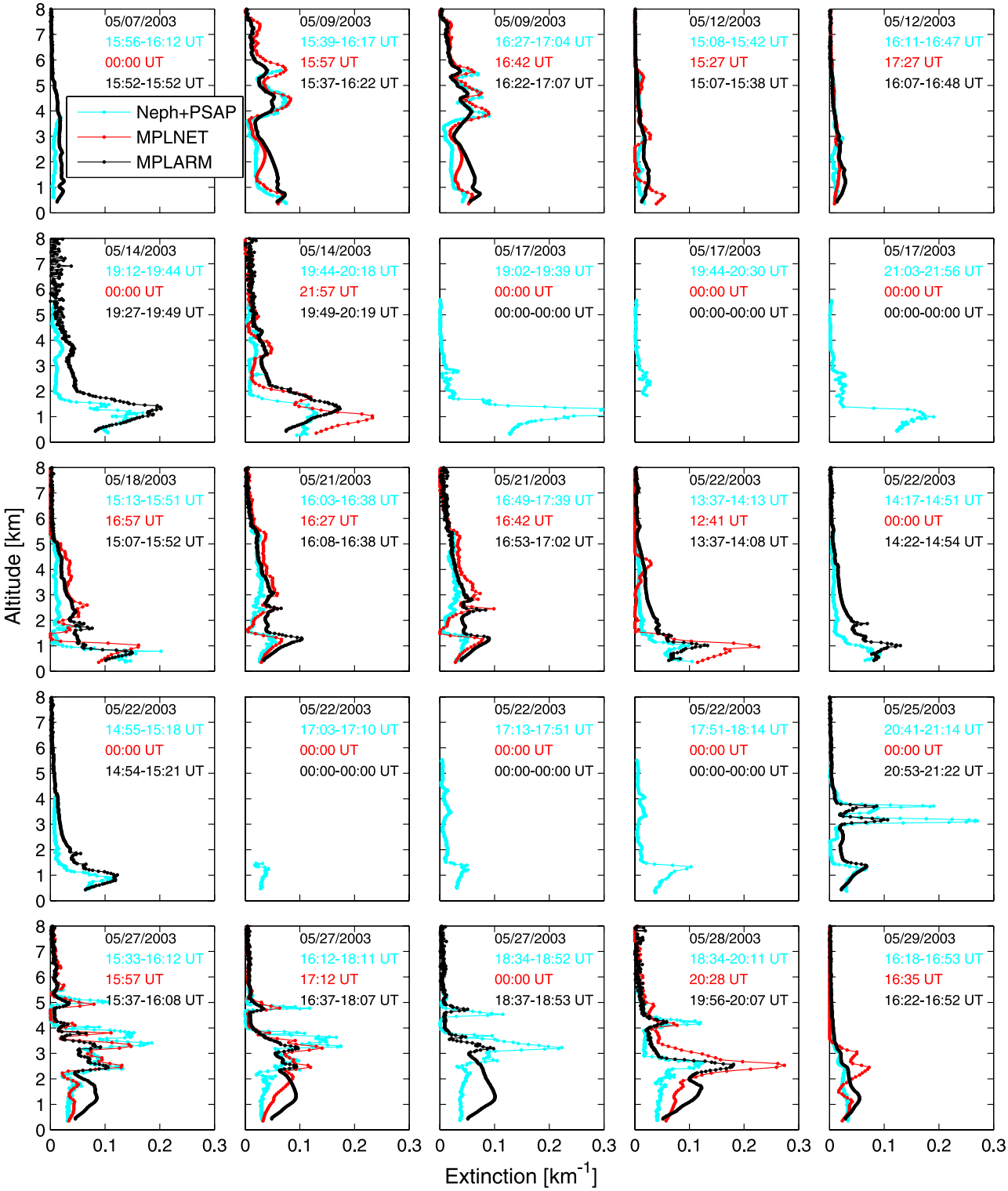

Figure 11. Vertical profiles of σ_{ep} from Nephelometer+PSAP (519 nm), MPLNET (523 nm), and MPLARM (523 nm) for the cases shown in Figure 2.

similar to what we found from low-altitude flybys over AERONET sites in previous campaigns. The agreement with a third ground-based Sun photometer (NIMFR) is particularly good (rms difference = 5%, bias = 1%, averaged over all λ), in fact operating four Sun photometers (including AATS-6) side-by-side on the ground in previous ARM IOPs did not result in a higher level of agreement.

[80] The robustness of the AATS-14 differentiated profiles of ρ_w and $\sigma_{ep}(\lambda)$ were tested by comparing ρ_w obtained from AATS-14 and the aircraft in situ sensors. This pre-

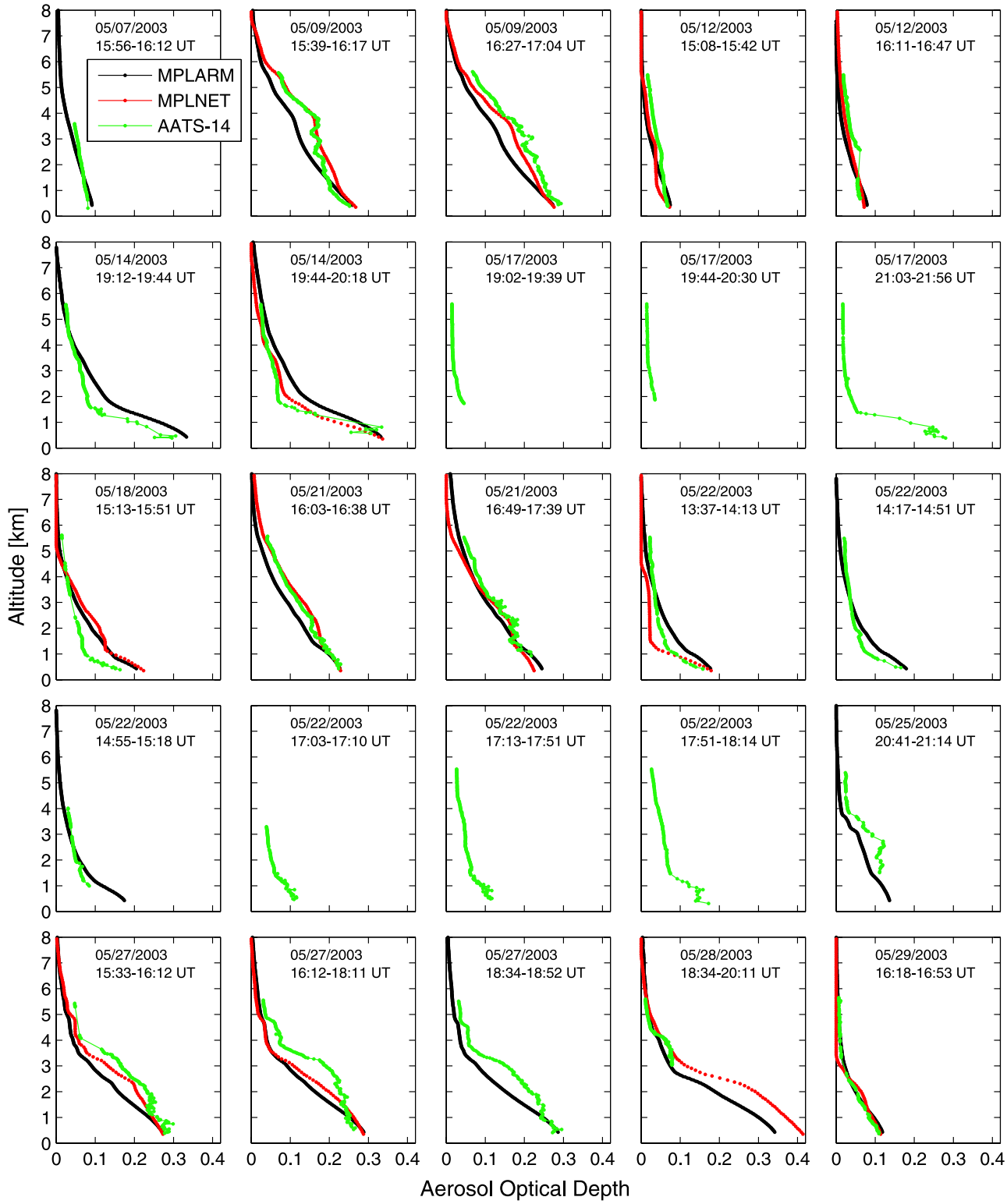

Figure 12. Vertical profiles of τ_p from MPLARM (523 nm), MPLNET (523 nm), and AATS-14 (519 nm) for the cases shown in Figure 2.

sumes that an aircraft in situ measurement of ρ_w is more straightforward than measuring ambient $\sigma_{ep}(\lambda)$. Averaged over 35 vertical profiles we find a relative RMS difference of 20% and a small bias difference of 5% (in situ ρ_w − AATS-14 ρ_w).

[81] Because most of the errors in AATS-14 $\tau_p(\lambda)$ or CWV are of systematic nature, they cancel out when differences (such as layer $\tau_p(\lambda)$ or LWV) or differentiations ($\sigma_{ep}(\lambda)$ or ρ_w) are used. However, uncertainties in the AATS-14 $\sigma_{ep}(\lambda)$ profiles arise from horizontal and temporal

Table 7. Comparison of Layer $\tau_p(\lambda)$ Between AATS-14 (or AATS-6) and Nephelometer+PSAP From Seven Campaigns

Campaign	Year	Location	Airplane	Study	n	r^2	λ, nm	Bias Difference, %
TARFOX	1996	U.S. east coast	U. Wash. C-131 A	*Hegg et al.* [1997]	14	0.904	450	−24
				Hartley et al. [2000]	11	0.963	450	−13
ACE-2	1997	Canary Islands	CIRPAS Pelican	*Schmid et al.* [2000]	2	n/a	450	−10
					2	n/a	530	−17
					2	n/a	700	−31
SAFARI 2000	2000	southern Africa	U. Wash CV-580	*Magi et al.* [2003]	15	0.982	550	−5
ACE-Asia	2001	eastern Asia	NCAR C-130	*Redemann et al.* [2003]	28	0.741	550	−4
			CIRPAS Twin Otter	*Schmid et al.* [2003b]	14	0.812	550	−9
CLAMS	2001	U.S. east coast	U. Wash CV-580	*Magi et al.* [2005]	14	0.931	550	−33
ARM AIOP	2003	Oklahoma	CIRPAS Twin Otter	this study	26	0.834	453	−16
					26	0.824	519	−18
					26	0.822	675	−21
							mean	−17

variability in the overlying aerosol. For the 25 $\sigma_{ep}(\lambda)$ vertical profiles used here this resulted in average $\delta\sigma_{ep}(\lambda = 453, 519, 675, 1558\ nm) = 0.032, 0.029, 0.024, 0.014\ \mathrm{Km}^{-1}$ equivalent to 101–176% if expressed as $\delta\sigma_{ep}(\lambda)/\sigma_{ep}(\lambda)$. The RMS differences (other methods versus AATS-14) in Table 3 are smaller than these uncertainties. One might therefore conclude that the $\sigma_{ep}(\lambda)$ measurements agree within the total error bars of AATS-14 alone. However, it is important to note, that the AATS-14 $\delta\sigma_{ep}(\lambda)$ represent random errors. It is possible to turn these random errors into bias errors for a single profile by flying a ramped ascent or descent under a pronounced aerosol gradient without changing heading. However, none of the profiles used in this study was acquired using such a flight pattern. Moreover, averaged over an ensemble of profiles (as done in this study) we can rule out a systematic bias due to spatial variability as this would require flying each profile with the pattern described above, under gradients with the same mathematical sign. The same discussion applies to the uncertainties of AATS-14 layer $\tau_p(\lambda)$ where, in fact, we observe differences that are often larger than the random errors (see Figure 10).

[82] Hence we believe the observed biases to be statistically significant. Furthermore, we find similar biases in the results published from previous field campaigns since 1996 involving AATS-6 or AATS-14:

[83] Combining the results from AIOP with those from 5 previous field campaigns, we find airborne Nephelometer+PSAP measurements of layer $\tau_p(\lambda = 450 - 700\ nm)$ to be biased slightly low (4–33%, average of 17%) when compared to airborne Sun photometer (AATS-6 or -14) values.

[84] From three previous campaigns we find layer $\tau_p(\lambda)$ calculated from airborne measurements of particle size distributions to be less than the AATS-6 or -14 values (average of 18%). However, the data set for this computationally involved comparison is relatively small.

[85] In 5 previous field campaigns we have compared $\sigma_{ep}(\lambda)$ and $\tau_p(\lambda)$ vertical profiles from one of the AATS instruments with surface based or airborne lidars. Many comparisons result in small or no biases, however the biases that do occur are positive (i.e., lidar $\sigma_{ep}(\lambda)$ larger than AATS values).

[86] There is a clear tendency for the remote sensing methods, lidar and airborne Sun photometers, to yield larger $\sigma_{ep}(\lambda)$ and $\tau_p(\lambda)$ values than the in situ methods. Adding the not previously used airborne cavity ring-down technique (Cadenza instrument), did not significantly alter that tendency. In fact, Cadenza's ability to in situ measure σ_{ep} at $\lambda = 1550$ nm, highlights the spectral signature of the low bias (i.e., low bias with respect to AATS-14 increases with increasing wavelength). We find the low bias of Neph+PSAP and Cadenza to be well correlated with ambient RH whereas its sensitivity to AATS-14 α_{ep} (a proxy for particle size) is obvious only in the Cadenza data. For the visible (but not for the near-infrared) wavelengths larger and spectrally dependent growth exponents γ that are in line with ground-based observations at SGP would eliminate the observed bias. It is likely though, that the low bias is caused by a combination of particle sampling losses and incomplete corrections for shrinkage by evaporation of water, organics, or nitrates.

[87] We cite numerous studies, with no AATS involved, that also found the remote sensing methods (lidar and Sun photometers) to yield larger $\sigma_{ep}(\lambda)$ or $\tau_p(\lambda)$ values than the in situ methods.

[88] Unknown gaseous absorption in the atmosphere (as postulated by *Halthore et al.* [1998]), not accounted for in the analysis of the Sun photometer and lidar data, could also lead to the observed biases. However, *Mlawer et al.* [2000]

Table 8. Comparison of Layer $\tau_p(\lambda)$ Measured With AATS-14 (or AATS-6) and Calculated From Size Distributions

Campaign	Year	Location	Airplane	Study	n	r^2	λ, nm	Bias Difference, %
TARFOX	1996	U.S. east coast	U. Wash. C-131 A	*Redemann et al.* [2000]	2	n/a	525	−39
ACE-2	1997	Canary Islands	CIRPAS Pelican	*Schmid et al.* [2000], *Collins et al.* [2000]	2	n/a	550	−9
ACE-Asia	2001	eastern Asia	CIRPAS Twin Otter	*Schmid et al.* [2003b], *Wang et al.* [2002]	4	n/a	550	−7
							mean	−18

Table 9. Comparison of Extinction Measured With Airborne AATS-14 (or AATS-6) and Lidars From Six Campaigns

Campaign	Year	Location	Study	x	y	λ(nm)	bias
TARFOX	1996	U.S. east coast	*Ferrare et al.* [2000]	AATS-6	GSFC SRL (ground)	355	positive
			Ferrare et al. [2000]	AATS-6	LASE (ER-2 aircraft)	815	slightly positive
ACE-2	1997	Canary Islands	*Schmid et al.* [2000], *Welton et al.* [2000]	AATS-14	MPL (ground)	523	neutral
			Livingston et al. [2000]	AATS-14	LMU (ship)	525	positive
PRIDE	2000	Caribbean	*Livingston et al.* [2003]	AATS-6	MPLNET (ground)	525	positive
SAFARI 2000	2001	southern Africa	*Schmid et al.* [2003a]	AATS-14	CPL (ER-2 aircraft)	532	slightly positive
			McGill et al. [2002]			1064	neutral
			Kaufman et al. [2003]		MPLNET (ground)	523	neutral
ACE-Asia	2001	eastern Asia	*Murayama et al.* [2003]	AATS-6	TUMM RL (ground)	532	n/a
ARM AIOP	2003	Oklahoma	this study, *Ferrare et al.* [2006]	AATS-14	CARL (ground)	355	54%
					MPLNET (ground)	523	13%
					MPLARM (ground)	523	24%

provide "strong evidence that in this spectral range [350–1000 nm] there are no unmodeled molecular absorbers of significance to the atmospheric energy balance."

[89] While we find that each of the methods investigated here has its strengths and weaknesses, there is no definitive proof that one of the methods is fundamentally flawed. From the biases found in AIOP and previous studies, we conclude that the systematic error associated with measuring the tropospheric vertical profile of the ambient aerosol extinction with current state-of-the-art instrumentation is 15–20% at visible wavelengths and potentially larger in the UV and near-infrared. Random errors, as measured by RMS differences (e.g., Table 3), are considerably larger, ranging from 26% to 98%.

Notation

AATS-6, -14 Ames Airborne Tracking (6)14-channel Sun photometer.
AERONET Aerosol Robotic Network.
ARM Atmospheric Radiation Measurement.
AIOP Aerosol Intensive Operations Period.
CARL CRF Raman lidar.
CRD cavity ring-down.
CRF Climate Research Facility.
CWV columnar water vapor.
FOV field of view.
IAP in situ aerosol profiles.
LWV layer water vapor.
MPL micropulse lidar.
NIMFR Normal Incidence Multifilter Radiometer.
p pressure.
PSAP Particle/Soot Absorption Photometer.
RH relative humidity.
SGP Southern Great Plains.
S_p extinction-to-backscatter ratio.
T temperature.
T_d dew point temperature.
V_0 Sun photometer calibration constant.
α_τ Ångström exponent of τp.
α_{ep} Ångström exponent of σep.
α_{sp} Ångström exponent of σsp.
γ humidification growth exponent.
δ uncertainty.
ρ_w water vapor density.
σ_{ap} aerosol absorption coefficient.
σ_{ep} aerosol extinction coefficient.
σ_{sp} aerosol scattering coefficient.
τ_p aerosol optical depth.

[90] **Acknowledgments.** The Atmospheric Radiation Measurement (ARM) Program is sponsored by the U.S. Department of Energy, Office of Science, Office of Biological and Environmental Research, Environmental Sciences Division. The success of the Aerosol IOP was due to the hard work and dedicated efforts from a large team of scientists and investigators from National Laboratories and Universities, CIRPAS Twin Otter and Cessna pilots, crew and support personnel, SGP site personnel, ARM infrastructure support, weather forecaster, and support from Greenwood aviation at Ponca City airport. We thank ARM for the support of this IOP. This research was also supported by a grant from the NOAA Office of Global Programs. E.J.W. and MPLNET are supported by the NASA Radiation Sciences Program and Earth Observing System. The authors would like to thank Jack Ji for operating AERONET and MPLNET instrumentation.

References

Ackerman, A. S., O. B. Toon, D. E. Stevens, A. J. Heymsfield, V. Ramanathan, and E. J. Welton (2000), Reduction of tropical cloudiness by soot, *Science*, *288*, 1042–1047.
Ackerman, T., and G. Stokes (2003), The Atmospheric Radiation Measurement Program, *Phys. Today*, *56*, 38–45.
Ackermann, J. (1998), The extinction-to-backscatter ratio of tropospheric aerosol: A numerical study, *J. Atmos. Oceanic Technol.*, *15*, 1043–1050.
Anderson, T. L., and J. A. Ogren (1998), Determining aerosol radiative properties using the TSI 3563 integrating nephelometer, *Aerosol Sci. Technol.*, *29*, 57–69.
Anderson, T. L., et al. (1996), Performance characteristics of a high-sensitivity, three wavelength, total scatter/backscatter nephelometer, *J. Atmos. Oceanic Technol.*, *13*, 967–986.
Anderson, T. L., S. J. Masonis, D. S. Covert, N. C. Ahlquist, S. G. Howell, A. D. Clarke, and C. S. McNaughton (2003), Variability of aerosol optical properties derived from in situ aircraft measurements during ACE-Asia, *J. Geophys. Res.*, *108*(D23), 8647, doi:10.1029/2002JD003247.
Andrews, E., P. J. Sheridan, J. A. Ogren, and R. Ferrare (2004), In situ aerosol profiles over the Southern Great Plains CART site: 1. Aerosol optical properties, *J. Geophys. Res.*, *109*, D06208, doi:10.1029/2003JD004025.
Andrews, E., et al. (2006), Comparison of methods for deriving aerosol asymmetry parameter, *J. Geophys. Res.*, *111*, D05S04, doi:10.1029/2004JD005734.
Ansmann, A., M. Riebesell, and C. Weitkamp (1990), Measurement of atmospheric aerosol extinction profiles with a Raman lidar, *Opt. Lett.*, *15*(13), 746–748.
Ansmann, A., et al. (2003), Long-range transport of Saharan dust to northern Europe: The 11–16 October 2001 outbreak observed with EARLINET, *J. Geophys. Res.*, *108*(D24), 4783, doi:10.1029/2003JD003757.
Bane, J. M., R. Bluth, C. Flagg, H. Jonsson, W. K. Melville, M. Prince, and D. Riemer (2004), UNOLS now oversees research aircraft facilities for ocean science, *Eos Trans. AGU*, *85*(41), 402.
Bluth, R. T., P. A. Durkee, J. H. Seinfeld, R. C. Flagan, L. M. Russell, P. A. Crowley, and P. Finn (1996), Center for Interdisciplinary Remotely-Piloted Aircraft Studies (CIRPAS), *Bull. Am. Meteorol. Soc.*, *77*, 2691–2699.

Bögel, W. (1977), Neue Näherungsgleichungen für den Sättigungsdruck des Wasserdampfes und für die in der Meteorologie gebräuchlichen Luftfeuchte-Parameter, *DLR-FB 77-52*, Dtsch. Forsch. und Versuchsanst. für Luft- und Raumfahrt, Oberpfaffenhofen, Germany.

Bond, T. C., T. L. Anderson, and D. Campbell (1999), Calibration and intercomparison of filter-based measurements of visible light absorption by aerosols, *Aerosol Sci. Technol.*, *30*, 582–600.

Bucholtz, A., et al. (2003), Properties and effects of Asian aerosols over the central California coast during the ADAM-2003 (Asian Dust Above Monterey-2003) field study, paper presented at 2003 Annual Conference, Am. Assoc. for Aerosol Res., Anaheim, Calif., 20–24 Oct.

Busch, K. W., and M. A. Busch (1999), *Cavity Ringdown Spectroscopy*, Am. Chem. Soc., Washington, D. C.

Campbell, J. R., D. L. Hlavka, E. J. Welton, C. J. Flynn, D. D. Turner, J. D. Spinhirne, V. S. Scott, and I. H. Hwang (2002), Full-time, eye-safe cloud and aerosol lidar observations at Atmospheric Radiation Measurement program sites: Instruments and data processing, *J. Atmos. Oceanic Technol.*, *19*, 431–442.

Chameides, W. L., and M. Bergin (2002), Soot takes center stage, *Science*, *297*, 2214–2215.

Chu, D. A., Y. J. Kaufman, G. Zibordi, J. D. Chern, J. Mao, C. Li, and B. N. Holben (2003), Global monitoring of air pollution over land from the Earth Observing System-Terra Moderate Resolution Imaging Spectroradiometer (MODIS), *J. Geophys. Res.*, *108*(D21), 4661, doi:10.1029/2002JD003179.

Clarke, A. D., J. N. Porter, F. P. J. Valero, and P. Pilweskie (1996), Vertical profiles, aerosol microphysics, and optical closure during the Atlantic Stratocumulus Transition Experiment: Measured and modeled column optical properties, *J. Geophys. Res.*, *101*, 4443–4453.

Clough, S. A., and M. J. Iacono (1995), Line-by-line calculations of atmospheric fluxes and cooling rates: 2. Application to carbon dioxide, ozone, methane, nitrous oxide, and the halocarbons, *J. Geophys. Res.*, *100*, 16,519–16,535.

Collins, D. R., et al. (2000), In situ aerosol size distributions and clear column radiative closure during ACE-2, *Tellus, Ser. B*, *52*, 498–525.

Damoah, R., N. Spichtinger, C. Forster, P. James, I. Mattis, U. Wandinger, S. Beirle, T. Wagner, and A. Stohl (2004), Around the world in 17 days—Hemispheric-scale transport of forest fire smoke from Russia in May 2003, *Atmos. Chem. Phys.*, *4*, 1311–1321.

Delene, D. J., and J. A. Ogren (2002), Variability of aerosol optical properties at four North American surface monitoring sites, *J. Atmos. Sci.*, *59*, 1135–1150.

Diner, D. J., W. A. Abdou, J. E. Conel, K. A. Crean, B. J. Gaitley, M. Helmlinger, R. A. Kahn, J. V. Martonchik, S. H. Pilorz, and B. N. Holben (2001), MISR aerosol retrievals over southern Africa during the SAFARI-2000 dry season campaign, *Geophys. Res. Lett.*, *28*, 3127–3130.

Eck, T. F., B. N. Holben, J. S. Reid, O. Dubovik, A. Smirnov, N. T. O'Neill, I. Slutsker, and S. Kinne (1999), Wavelength dependence of the optical depth of biomass burning, urban, and desert dust aerosols, *J. Geophys. Res.*, *104*, 31,333–31,349.

Ferrare, R., et al. (2000), Comparisons of aerosol optical properties and water vapor among ground and airborne lidars and sun photometers during TARFOX, *J. Geophys. Res.*, *105*(D8), 9917–9933.

Ferrare, R. A., D. D. Turner, L. A. Heilman, W. Feltz, O. Dubovik, and T. Tooman (2001), Raman lidar measurements of the aerosol extinction-to-backscatter ratio over the Southern Great Plains, *J. Geophys. Res.*, *106*, 20,333–20,347.

Ferrare, R. A., et al. (2003), Vertical variability of aerosols and water vapor over the Southern Great Plains, paper presented at DOE ARM Science Team Meeting, U.S. Dep. of Energy, Broomfield, Colo. (Available at http://www.arm.gov/publications/proceedings/conf13/extended_abs/ferrare-ra.pdf)

Ferrare, R., et al. (2006), Evaluation of daytime measurements of aerosols and water vapor made by an operational Raman lidar over the Southern Great Plains, J. Geophys. Res., *111*, D05S08 doi:10.1029/2005JD005836.

Gassó, S., et al. (2000), Influence of humidity on the aerosol scattering coefficient and its effect on the upwelling radiance during ACE-2, *Tellus, Ser. B*, *52*, 546–567.

Hallar, A. G., et al. (2006), ARM Aerosol Intensive Operating Period: Comparison of aerosol scattering during coordinated flights, *J. Geophys. Res.*, doi:10.1029/2005JD006250, in press.

Halthore, R. N., S. Nemesure, S. E. Schwartz, D. G. Imre, A. Berk, E. G. Dutton, and M. H. Bergin (1998), Models overestimate diffuse clear-sky surface irradiance: A case for excess atmospheric absorption, *Geophys. Res. Lett.*, *25*(19), 3591–3594.

Hansen, J., M. Sato, R. Ruedy, A. Lacis, and V. Oinas (2000), Global warming in the twenty-first century: An alternative scenario, *Proc. Natl. Acad. Sci. U.S.A.*, *97*, 9875–9880.

Harder, J. W., J. W. Brault, P. V. Johnston, and G. H. Mount (1997), Temperature dependent NO_2 cross sections at high spectral resolution, *J. Geophys. Res.*, *102*, 3861–3879.

Harrison, L., J. Michalsky, and J. Berndt (1994), Automated multifilter rotating shadow-band radiometer: an instrument for optical depth and radiation measurements, *Appl. Opt.*, *33*(22), 5118–5125.

Hartley, W. S., P. V. Hobbs, J. L. Ross, P. B. Russell, and J. M. Livingston (2000), Properties of aerosols aloft relevant to direct radiative forcing off the mid-Atlantic coast of the United States, *J. Geophys. Res.*, *105*(D8), 9859–9886.

Hegg, D. A., J. Livingston, P. V. Hobbs, T. Novakov, and P. Russell (1997), Chemical apportionment of aerosol column optical depth off the mid-Atlantic coast of the United States, *J. Geophys. Res.*, *102*(D21), 25,293–25,303.

Hegg, D. A., D. S. Covert, H. Jonsson, and P. A. Covert (2005), Determination of the transmission efficiency of an aircraft aerosol inlet, *Aerosol Sci. Technol.*, *39*(10), 966–971.

Holben, B. N., et al. (1998), AERONET—A federated instrument network and data archive for aerosol characterization, *Remote Sens. Environ.*, *66*, 1–16.

Holben, B. N., et al. (2001), An emerging ground-based aerosol climatology: Aerosol Optical Depth from AERONET, *J. Geophys. Res.*, *106*, 12,067–12,097.

Jacobson, M. Z. (2002), Control of fossil-fuel particulate black carbon and organic matter, possibly the most effective method of slowing global warming, *J. Geophys. Res.*, *107*(D19), 4410, doi:10.1029/2001JD001376.

Kasten, F. (1969), Visibility in the phase of pre-condensation, *Tellus*, *21*, 631–635.

Kato, S., et al. (2000), A comparison of the aerosol optical thickness derived from ground-based and airborne measurements, *J. Geophys. Res.*, *105*(D11), 14,701–14,717.

Kaufman, Y., D. Tanré, and O. Boucher (2002), A satellite view of aerosols in the climate system, *Nature*, *419*, 215–223.

Kaufman, Y. J., J. M. Haywood, P. V. Hobbs, W. Hart, R. Kleidman, and B. Schmid (2003), Remote sensing of vertical distributions of smoke aerosol off the coast of Africa during SAFARI 2000, *Geophys. Res. Lett.*, *30*(16), 1831, doi:10.1029/2003GL017068.

King, M. D., and D. M. Byrne (1976), A method for inferring total ozone content from the spectral variation of total optical depth obtained with a solar radiometer, *J. Atmos. Sci.*, *33*, 2242–2251.

Kotchenruther, R. A., P. V. Hobbs, and D. A. Hegg (1999), Humidification factors for atmospheric aerosols off the mid-Atlantic coast of the United States, *J. Geophys. Res.*, *104*(D2), 2239–2251.

Lelieveld, J., et al. (2002), Global air pollution crossroads over the Mediterranean, *Science*, *298*, 794–799.

Livingston, J. M., et al. (2000), Shipboard Sun photometer measurements of aerosol optical depth spectra and columnar water vapor during ACE 2 and comparison to selected land, ship, aircraft, and satellite measurements, *Tellus, Ser. B*, *52*, 594–619.

Livingston, J. M., et al. (2003), Airborne Sun photometer measurements of aerosol optical depth and columnar water vapor during the Puerto Rico Dust Experiment, and comparison with land, aircraft, and satellite measurements, *J. Geophys. Res.*, *108*(D19), 8588, doi:10.1029/2002JD002520.

Livingston, J. M., et al. (2005), Retrieval of ozone column content from airborne Sun photometer measurements during SOLVE II: Comparison with coincident satellite and aircraft measurements, *Atmos. Chem. Phys. Disc.*, *5*, 243–286.

Magi, B. I., P. V. Hobbs, B. Schmid, and J. Redemann (2003), Vertical profiles of light scattering, light absorption and single scattering albedo during the dry, biomass burning season in southern Africa and comparisons of in situ and remote sensing measurements of aerosol optical depths, *J. Geophys. Res.*, *108*(D13), 8504, doi:10.1029/2002JD002361.

Magi, B. I., P. V. Hobbs, D. A. Hegg, T. W. Kirchstetter, T. Novakov, S. Gao, J. Redemann, and B. Schmid (2005), Aerosol properties and chemical apportionment of aerosol optical depth at locations off the United States east coast in July and August 2001, *J. Atmos. Sci.*, *62*(4), 919–933, doi:10.1175/JAS3263.1.

Masonis, S. J., K. Franke, A. Ansmann, D. Muller, D. Althausen, J. A. Ogren, A. Jefferson, and P. J. Sheridan (2002), An intercomparison of aerosol light extinction and 180°-backscatter as derived using in situ instruments and Raman lidar during the INDOEX field campaign, *J. Geophys. Res.*, *107*(D19), 8014, doi:10.1029/2000JD000035.

Matsumoto, T., P. B. Russell, C. Mina, W. Van Ark, and V. Banta (1987), Airborne tracking Sun photometer, *J. Atmos. Oceanic Technol.*, *4*, 336–339.

McGill, M., D. Hlavka, W. Hart, J. Spinhirne, S. Scott, and B. Schmid (2002), The cloud physics lidar: Instrument description and initial measurement results, *Appl. Opt.*, *41*(18), 3725–3734.

Menon, S., J. Hansen, L. Nazarenko, and Y. Luo (2002), Climate effects of black carbon aerosols in China and India, *Science*, *297*, 2250–2252.

Mlawer, E. J., P. D. Brown, S. A. Clough, L. C. Harrison, J. J. Michalsky, P. W. Kiedron, and T. Shippert (2000), Comparison of spectral direct and diffuse solar irradiance measurements and calculations for cloud-free conditions, *Geophys. Res. Lett.*, *27*, 2653–2656.

Murayama, T., et al. (2003), An intercomparison of lidar-derived aerosol optical properties with airborne measurements near Tokyo during ACE-Asia, *J. Geophys. Res.*, *108*(D23), 8651, doi:10.1029/2002JD003259.

O'Keefe, A., and D. A. G. Deacon (1988), Cavity ring-down optical spectrometer for absorption measurements using pulsed laser sources, *Rev. Sci. Instrum.*, *59*, 2544–2551.

Penner, J. E. (2003), Comment on "Control of fossil-fuel particulate black carbon and organic matter, possibly the most effective method of slowing global warming" by M. Z. Jacobson, *J. Geophys. Res.*, *108*(D24), 4771, doi:10.1029/2002JD003364.

Penner, J. E., S. Y. Zhang, and C. C. Chuang (2003), Soot and smoke aerosol may not warm climate, *J. Geophys. Res.*, *108*(D21), 4657, doi:10.1029/2003JD003409.

Petzold, A., M. Fiebig, H. Flentje, A. Keil, U. Leiterer, F. Schröder, A. Stifter, M. Wendisch, and P. Wendling (2002), Vertical variability of aerosol properties observed at a continental site during the Lindenberg Aerosol Characterization Experiment (LACE 98), *J. Geophys. Res.*, *107*(D21), 8128, doi:10.1029/2001JD001043.

Ramanathan, V., P. J. Crutzen, J. T. Kiehl, and D. Rosenfeld (2001), Aerosol, climate and the hydrological cycle, *Science*, *294*, 2119–2124.

Redemann, J., et al. (2000), Retrieving the vertical structure of the effective aerosol complex index of refraction from a combination of aerosol in situ and remote sensing measurements during TARFOX, *J. Geophys. Res.*, *105*(D8), 9949–9970.

Redemann, J., P. B. Russell, and P. Hamill (2001), Dependence of aerosol light absorption and single-scattering albedo on ambient relative humidity for sulfate aerosols with black carbon cores, *J. Geophys. Res.*, *106*, 27,485–27,495.

Redemann, J., S. J. Masonis, B. Schmid, T. L. Anderson, P. B. Russell, J. M. Livingston, O. Dubovik, and A. D. Clarke (2003), Clear-column closure studies of aerosols and water vapor aboard the NCAR C-130 during ACE-Asia, 2001, *J. Geophys. Res.*, *108*(D23), 8655, doi:10.1029/2003JD003442.

Redemann, J., B. Schmid, J. A. Eilers, R. Kahn, R. C. Levy, P. B. Russell, J. M. Livingston, P. V. Hobbs, W. L. Smith Jr., and B. N. Holben (2005), Suborbital measurements of spectral aerosol optical depth and its variability at sub-satellite-grid scales in support of CLAMS, 2001, *J. Atmos. Sci.*, *62*(4), 993–1007, doi:10.1175/JAS3387.1.

Remer, L. A., S. Gassó, D. A. Hegg, Y. J. Kaufman, and B. N. Holben (1997), Urban/industrial aerosol: Ground-based Sun/sky radiometer and airborne in situ measurements, *J. Geophys. Res.*, *102*(D14), 16,849–16,859.

Rothman, L. S., and J. Schroeder (2002), Millennium HITRAN compilation, paper presented at 12th ARM Science Team Meeting, U.S. Dep. of Energy, St. Petersburg, Fla., 8–12 April.

Rothman, L. S., K. Chance, J. Schroeder, and A. Goldman (2001), New edition of HITRAN database, paper presented at 11th ARM Science Team Meeting, U.S. Dep. of Energy, Atlanta, Ga., 19–23 March.

Rotstayn, L. D., and U. Lohmann (2002), Tropical rainfall trends and the indirect aerosol effect, *J. Clim.*, *15*, 2103–2116.

Russell, P. B., et al. (1993a), Pinatubo and pre-Pinatubo optical-depth spectra: Mauna Loa measurements, comparisons, inferred particle size distributions, radiative effects, and relationship to lidar data, *J. Geophys. Res.*, *98*, 22,969–22,985.

Russell, P. B., et al. (1993b), Post-Pinatubo optical depth spectra vs. latitude and vortex structure: Airborne tracking Sun photometer measurements in AASE II, *Geophys. Res. Lett.*, *20*, 2571–2574.

Russell, P. B., P. V. Hobbs, and L. L. Stowe (1999a), Aerosol properties and radiative effects in the United States mid-Atlantic haze plume: An overview of the Tropospheric Aerosol Radiative Forcing Observational Experiment (TARFOX), *J. Geophys. Res.*, *104*, 2213–2222.

Russell, P. B., J. M. Livingston, P. Hignett, S. Kinne, J. Wong, and P. V. Hobbs (1999b), Aerosol-induced radiative flux changes off the United States Mid-Atlantic coast: Comparison of values calculated from Sun photometer and in situ data with those measured by airborne pyranometer, *J. Geophys. Res.*, *104*, 2289–2307.

Russell, P. B., J. M. Livingston, O. Dubovik, S. A. Ramirez, J. Wang, J. Redemann, B. Schmid, M. Box, and B. N. Holben (2004), Sunlight transmission through desert dust and marine aerosols: Diffuse light corrections to Sun photometry and pyrheliometry, *J. Geophys. Res.*, *109*, D08207, doi:10.1029/2003JD004292.

Russell, P., et al. (2005), Aerosol optical depth measurements by airborne Sun photometer in SOLVE II: Comparisons to SAGE III, POAM III and airborne spectrometer measurements, *Atmos. Chem. Phys.*, *5*, 1311–1339.

Sato, M., J. Hansen, D. Koch, A. Lacis, R. Ruedy, O. Dubovik, B. Holben, M. Chin, and T. Novakov (2003), Global atmospheric black carbon inferred from AERONET, *Proc. Natl. Acad. Sci. U. S. A.*, *100*, 6319–6324.

Schmid, B., and C. Wehrli (1995), Comparison of sun photometer calibration by Langley technique and standard lamp, *Appl. Opt.*, *34*, 4500–4512.

Schmid, B., K. J. Thome, P. Demoulin, R. Peter, C. Mätzler, and J. Sekler (1996), Comparison of modeled and empirical approaches for retrieving columnar water vapor from solar transmittance measurements in the 0.94 micron region, *J. Geophys. Res.*, *101*, 9345–9358.

Schmid, B., C. Mätzler, A. Heimo, and N. Kämpfer (1997), Retrieval of optical depth and size distribution of tropospheric and stratospheric aerosols by means of Sun photometry, *IEEE Trans. Geosci. Remote Sens.*, *35*(1), 172–182.

Schmid, B., P. R. Spyak, S. F. Biggar, C. Wehrli, J. Sekler, T. Ingold, C. Mätzler, and N. Kämpfer (1998), Evaluation of the applicability of solar and lamp radiometric calibrations of a precision Sun photometer operating between 300 and 1025 nm, *Appl. Opt.*, *37*, 3923–3941.

Schmid, B., J. Michalsky, R. Halthore, M. Beauharnois, L. Harrison, J. Livingston, P. Russell, B. Holben, T. Eck, and A. Smirnov (1999), Comparison of aerosol optical depth from four solar radiometers during the Fall 1997 ARM Intensive Observation Period, *Geophys. Res. Lett.*, *26*(17), 2725–2728.

Schmid, B., et al. (2000), Clear sky closure studies of lower tropospheric aerosol and water vapor during ACE 2 using airborne Sun photometer, airborne in-situ, space-borne, and ground-based measurements, *Tellus, Ser. B*, *52*, 568–593.

Schmid, B., et al. (2001), Comparison of columnar water-vapor measurements from solar transmittance methods, *Appl. Opt.*, *40*, 1886–1896.

Schmid, B., et al. (2003a), Coordinated airborne, spaceborne, and ground-based measurements of massive, thick aerosol layers during the dry season in southern Africa, *J. Geophys. Res.*, *108*(D13), 8496, doi:10.1029/2002JD002297.

Schmid, B., et al. (2003b), Column closure studies of lower tropospheric aerosol and water vapor during ACE-Asia using airborne Sun photometer, airborne in-situ and ship-based lidar measurements, *J. Geophys. Res.*, *108*(D23), 8656, doi:10.1029/2002JD003361.

Sheridan, P. J., D. J. Delene, and J. A. Ogren (2001), Four years of continuous surface aerosol measurements from the Department of Energy's Atmospheric Radiation Measurement Program Southern Great Plains Cloud and Radiation Testbed site, *J. Geophys. Res.*, *106*(D18), 20,735–20,747.

Sheridan, P. J., et al. (2005), The Reno Aerosol Optics Study: An evaluation of aerosol absorption measurement methods, *Aerosol Sci. Technol.*, *39*(1), 1–16, doi:10.1080/027868290901891.

Sivaraman, C., D. D. Turner, and C. J. Flynn (2004), Techniques and methods used to determine the aerosol best estimate value-added product at the SGP central facility, paper presented at 14th ARM Science Team Meeting, U.S. Dep. of Energy, Albuquerque, N. M. (Available at http://www.arm.gov/publications/proceedings/conf14/extended_abs/sivaraman-c.pdf)

Smirnov, A. (2004), AERONET processing algorithms refinement, paper presented at AERONET Workshop, NASA, El Arenosillo, Spain, 10–14 May.

Smirnov, A., B. N. Holben, T. F. Eck, O. Dubovik, and I. Slutsker (2000), Cloud-screening and quality control algorithms for the AERONET database, *Remote Sens. Environ.*, *73*, 337–349.

Smith, J. D., and D. B. Atkinson (2001), A portable pulsed cavity ring-down transmissometer for measurement of the optical extinction of the atmospheric aerosol, *Analyst*, *126*(8), 1216–1220.

Spinhirne, J. D., J. A. R. Rall, and V. S. Scott (1995), Compact eye safe lidar systems, *Rev. Laser Eng.*, *23*, 112–118.

Spinhirne, J. D., S. P. Palm, W. D. Hart, D. L. Hlavka, and E. J. Welton (2005), Cloud and aerosol measurements from GLAS: Overview and initial results, *Geophys. Res. Lett.*, *32*, L22S03, doi:10.1029/2005GL023507.

Sprent, P., and G. Dolby (1980), The geometric mean functional relationship, *Biometrics*, *36*, 547–550.

Strawa, A. W., R. Castaneda, T. Owano, D. S. Baer, and B. A. Paldus (2003), The measurement of aerosol optical properties using continuous wave cavity ring-down techniques, *J. Atmos. Oceanic Technol.*, *20*, 454–465.

Strawa, A. W., et al. (2006), In situ measurement of aerosol optical properties made during the DOE Aerosol IOP: 1. Comparison of extinction and scattering coefficients, *J. Geophys. Res.*, doi:10.1029/2005JD006056, in press.

Torres, O., P. K. Bhartia, J. R. Herman, A. Sinyuk, P. Ginoux, and B. Holben (2002), A long-term record of aerosol optical depth from TOMS observations and comparison to AERONET measurements, *J. Atmos. Sci.*, *59*, 398–413.

Turner, D. D., R. A. Ferrare, and L. A. Brasseur (2001), Average aerosol extinction and water vapor profiles over the Southern Great Plains, *Geophys. Res. Lett.*, *28*, 4441–4444.

Turner, D. D., R. A. Ferrare, L. A. Heilman, W. F. Feltz, and T. Tooman (2002), Automated retrievals of water vapor and aerosol profiles over Oklahoma from an operational Raman lidar, *J. Atmos. Oceanic Technol.*, *19*, 37–50.

VanCuren, R. A. (2003), Asian aerosols in North America: Extracting the chemical composition and mass concentration of the Asian continental aerosol plume from long-term aerosol records in the western United States, *J. Geophys. Res.*, *108*(D20), 4623, doi:10.1029/2003JD003459.

Virkkula, A., N. C. Ahlquist, D. S. Covert, W. P. Arnott, P. J. Sheridan, P. K. Quinn, and D. J. Coffman (2005), Modification, calibration and a field test of an instrument for measuring light absorption by particles, *Aerosol Sci. Technol.*, *39*(1), 68–83, doi:10.1080/027868290901963.

Wang, J., et al. (2002), Clear-column radiative closure during ACE-Asia: Comparison of multiwavelength extinction derived from particle size and composition with results from sunphotometry, *J. Geophys. Res.*, *107*(D23), 4688, doi:10.1029/2002JD002465.

Wang, J., S. A. Christopher, U. S. Nair, J. S. Reid, E. M. Prins, J. Szykman, and J. L. Hand (2006), Mesoscale modeling of Central American smoke transport to the United States: "Top-down" assessment of emission strength and diurnal variation impacts, *J. Geophys. Res.*, doi:10.1029/2005JD006416, in press.

Welton, E. J., et al. (2000), Ground-based lidar measurements of aerosols during ACE-2: Instrument description, results, and comparisons with other ground-based and airborne measurements, *Tellus, Ser. B*, *52*, 635–650.

Welton, E. J., J. R. Campbell, J. D. Spinhirne, and V. S. Scott (2001), Global monitoring of clouds and aerosols using a network of micro-pulse lidar systems, in *Lidar Remote Sensing for Industry and Environmental Monitoring*, edited by U. N. Singh, T. Itabe, and N. Sugimoto, *Proc. SPIE Int. Soc. Opt. Eng.*, *4153*, 151–158.

Welton, E. J., K. J. Voss, P. K. Quinn, P. J. Flatau, K. Markowicz, J. R. Campbell, J. D. Spinhirne, H. R. Gordon, and J. E. Johnson (2002), Measurements of aerosol vertical profiles and optical properties during INDOEX 1999 using micro-pulse lidars, *J. Geophys. Res.*, *107*(D19), 8019, doi:10.1029/2000JD000038.

J. Barnard and C. Flynn, Pacific Northwest National Laboratory, Richland, WA 99352, USA.

M. Clayton, SAIC/NASA Langley Research Center, Hampton, VA 23681, USA.

D. Covert and R. Elleman, Department of Atmospheric Sciences, University of Washington, Seattle, WA 98195, USA.

J. Eilers, A. G. Hallar, and A. Strawa, NASA Ames Research Center, Moffett Field, CA 94035, USA.

R. Ferrare, NASA Langley Research Center, Hampton, VA 23681, USA.

B. Holben and E. Welton, NASA Goddard Space Flight Center, Greenbelt, MD 20771, USA.

H. Jonsson, Center for Interdisciplinary Remotely-Piloted Aircraft Studies, Marina, CA 93633, USA.

J. Michalsky, NOAA Air Resources Laboratory, Boulder, CO 80305, USA.

J. Redemann and B. Schmid, Bay Area Environmental Research Institute, NASA Ames Research Center, MS 245-5, Moffett Field, CA 94035-1000, USA. (bschmid@mail.arc.nasa.gov)

K. Ricci, Los Gatos Research Inc., Mountain View, CA 94041-1529, USA.

A. Smirnov, Goddard Earth Science and Technology Center, University of Maryland Baltimore County/NASA Goddard Space Flight Center, Greenbelt, MD 20771, USA.

D. Turner, Space Science and Engineering Center, University of Wisconsin, Madison, WI 53706, USA.